

The Role of Actively Created Doppler shifts in Bats – Behavioral Experiments & Biomimetic Reproductions

Xiaoyan Yin

Dissertation submitted to the Faculty of the
Virginia Polytechnic Institute and State University
in partial fulfillment of the requirements for the degree of

Doctor of Philosophy
in
Mechanical Engineering

Rolf Müller, Chair

Nicole Abaid

Alexander Leonessa

Michael Roan

Jake Socha

December 16, 2020

Blacksburg, Virginia

Keywords: Bats | Biosonar | Pinna Motions | Doppler Shifts | Direction finding |

Biomimetics | Deep Learning

Copyright 2021, Xiaoyan Yin

The Role of Actively Created Doppler shifts in Bats – Behavioral Experiments & Biomimetic Reproductions

Xiaoyan Yin

(ABSTRACT)

Many animal species are known for their unparalleled abilities to encode sensory information that supports fast, reliable action in complex environments, but the mechanisms remain often unclear. Through fast ear motions, bats can encode information on target direction into time-frequency Doppler signatures. These species were thought to be evolutionarily tuned to Doppler shifts generated by a prey's wing beat. Self-generated Doppler shifts from the bat's own flight motion were for the most part considered a nuisance that the bats compensate for. My findings indicate that these Doppler-based biosonar systems may be more complicated than previously thought because the animals can actively inject Doppler shifts into their input signals. The work in this dissertation presents a novel nonlinear principle for sensory information encoding in bats. Up to now, sound-direction finding has required either multiple signal frequencies or multiple pressure receivers. Inspired by bat species that add Doppler shifts to their biosonar echoes through fast ear motions, I present a source-direction finding paradigm based on a single frequency and a single pressure receiver. Non-rigid ear motions produce complex Doppler signatures that depend on source direction but are difficult to interpret. To demonstrate that deep learning can solve this problem, I have combined a soft-robotic microphone baffle that mimics a deforming bat ear with a CNN for regression. With this integrated cyberphysical setup, I have able to achieve a direction-finding accuracy of 1 degree based on a single baffle motion.

The Role of Actively Created Doppler shifts in Bats – Behavioral Experiments & Biomimetic Reproductions

Xiaoyan Yin

(GENERAL AUDIENCE ABSTRACT)

Bats are well-known for their intricate biosonar system that allow the animals to navigate even the most complex natural environments. While the mechanism behind most of these abilities remains unknown, an interesting observation is that some bat species produce fast movements of their ears when actively exploring their surroundings. By moving their pinna, the bats create a time-variant reception characteristic and very little research has been directed at exploring the potential benefits of such behavior so far. One hypothesis is that the speed of the pinna motions modulates the received biosonar echoes with Doppler-shift patterns that could convey sensory information that is useful for navigation. This dissertation intends to explore this hypothetical dynamic sensing mechanism by building a soft-robotic biomimetic receiver to replicate the dynamics of the bat pinna. The experiments with this biomimetic pinna robot demonstrate that the non-rigid ear motions produce Doppler signatures that contain information about the direction of a sound source. However, these patterns are difficult to interpret because of their complexity. By combining the soft-robotic pinna with a convolutional neural network for processing the Doppler signatures in the time-frequency domain, I have been able to accurately estimate the source direction with an error margin of less than one degree. This working system, composed of a soft-robotic biomimetic ear integrated with a deep neural net, demonstrates that the use of Doppler signatures as a source of sensory information is a viable hypothesis for explaining the sensory skills of bats.

Dedication

I dedicate this dissertation to my father Zhengbao Yin and my mother Yuxiang Zhang, for their selfless love and unconditional support and who have always supported me in my pursuit of learning. To my sister Hang Yin who is always bringing laughs to the family.

Acknowledgments

First, I would like to express my heartfelt gratitude to my advisor Dr. Rolf Müller for having provided me this opportunity, his trust, timely guidance, continuous encouragement, and support throughout the entire duration of my Ph.D. studies. He taught me so much and his meticulous academic spirit and great passion to pursue science inspired me to be a better researcher. I could not have imagined having a better advisor for my Ph.D. study. Besides my advisor, I would also like to thank the rest of my thesis committee: Dr. Alexander Leonessa, Dr. Nicole Abaid, Dr. Michael Roan, and Dr. Jake Socha for their insightful comments on my Ph.D. research and continuous encouragement throughout my Ph.D. studies. I would like to acknowledge Philip Caspers who had built the first version of the soft-robotic pinna. I would also like to acknowledge Michael Goldsworthy for his help in the machine learning algorithms. I would also like to thank other lab colleagues, Joseph Sutlive, Ruihao Wang, Liujun Zhang, Ananya Bhardwaj, Shuxin Zhang, Peiwen Qiu, and Luhui Yang for the research discussions and the fun we had during my time in the lab. Finally, I would like to thank my loving family members, my parents Zhengbao Yin and Yuxiang Zhang, and my sister Hang Yin who encouraged me and were always there for help in my difficult times.

Contents

List of Figures	ix
1 Introduction	1
1.1 Bat Biosonar System	1
1.2 Emitter and Receiver Dynamics of Bats	5
1.3 Experimental Study of Biosonar Dynamics in Bats	7
1.4 Bat-inspired Sensing Systems	8
2 Discoveries in the Bat's Biosonar System	11
2.1 Title	11
2.2 Abstract	11
2.3 Introduction	12
2.4 Materials and Methods	13
2.4.1 Overall Experimental Setup and Animal Care	13
2.4.2 3D Reconstruction of Pinna Motions	14
2.4.3 Ultrasound Recording	15
2.4.4 Biomimetic Pinna Experiments	16
2.4.5 Data Sets and Processing	18

2.5	Results	24
2.5.1	Fast Pinna Motion Speed	24
2.5.2	Direction Between Motion and Echo	25
2.5.3	Motion Occur During Echo	26
2.5.4	Doppler Shift From Recording and Calculation are Matching	28
2.5.5	Doppler Shift Patterns	29
2.6	Discussion	29
3	Applications of the Soft Robotics	34
3.1	Title	34
3.2	Abstract	34
3.3	Introduction	35
3.4	Materials and Methods	37
3.4.1	Experimental Setup	37
3.4.2	Data Preprocessing	39
3.4.3	Convolutional Neural Network Training	40
3.4.4	Direction Estimation Testing	41
3.5	Results	42
3.5.1	Doppler-shift Signature Associated With Different Directions	42
3.5.2	Deep Learning of Direction Finding from Doppler Signatures	42

3.5.3 Accuracy of Direction Finding with the Dynamic Soft-robotic Pinna .	44
3.6 Discussion	46
4 Summary and Conclusions	48
4.1 Major Findings	48
4.2 Discussion	49
4.3 Suggestions for Future Work	51
Bibliography	52
Appendices	71
Appendix A Matlab Code for Spectrogram Extraction	72
Appendix B Python Code for CNN Training	75

List of Figures

2.1	Experimental setup for the animal experiments. A) example high-speed video frame showing the landmark points placed on the pinna rim (point numbers 1 to 15), noseleaf (point numbers 22 to 28), and head (point numbers 16 to 21) of a hipposiderid bat to facilitate motion capture B) setup consisting of an array of four high-speed video cameras, LED illumination from two directions, and an array of seven measurement microphones. High-speed cameras and microphone data acquisition were synchronized. C) 3D reconstructions of the motion trajectories of the points shown in (A). The arrow indicates the motion direction with time. The rim of the pinna and the end point of the motion shown on panel A).	14
2.2	Biomimetic pinna. A) overview of the device, B) motor and cam shaft, C) pinna holder with the artificial ear canal.	17
2.3	Doppler shifts received at the ear canal of biomimetic pinna. Power spectral density of the signal received in ear canal with (black lines) and without (gray lines) ear motions. Dashed lines show the standard deviations of the spectrum estimates ($N = 15$ for each condition).	20

2.4	Information-theoretic paradigm for finding an upper bound on the number of resolvable directions for biosonar targets: The method assumes that the direction (azimuth and elevation) space is divided into resolvable sub-regions. The estimate on the maximum number of resolvable regions does not make an assumption on the size and shape of the regions, hence they may not be uniform as depicted in the sketch shown here.	21
2.5	Doppler signatures created by ear motion. A) example of raw spectrogram, B) smoothed spectrogram (2-D Gaussian image filter with a mask size of 3 pixels and a standard deviation of 0.5 pixels).	22
2.6	Pinna tip speeds and maximum Doppler shifts for all three bat species studied. A) Pinna tip speeds calculated from reconstructed 3d trajectories of landmarks placed on the pinna tip. B) Maximum Doppler shifts calculated under the assumption that the pinna moves in the direction of sound propagation (center line: median, box edges: 25th and 75th percentiles, whiskers: minimum and maximum values). Maximum Doppler shifts were calculated under the assumption that the direction of the maximum pinna surface velocity is aligned with the radiation direction of the echoes.	25
2.7	Distribution of speed, directional cosine between surface velocity and radiation direction, and Doppler shift on the inner surface of the pinna. A) maximum surface speed during a pinna motion, B) directional cosine between surface velocity and the direction of sound propagation associated with the maximum speed, C) Doppler shift estimates based on A) and B). Directional cosines were calculated under the assumption that the propagation direction of the echo corresponds to the direction associated with the maximum amplitude of the pulse.	27

2.8 **Fast pinna motions and large Doppler shifts occur during echoes.**

A) Pinna surface speed calculated from the landmark on the tip of the pinna superimposed on the spectrogram of biosonar pulse from RF and its echoes. In shown example recording, the pulses coincided with a forward motion of the pinna (positive speeds). B) Portion of pulses with maximum Doppler shift exceeding a certain threshold. Number of motion sequences/echoes analyzed:

H. armiger: 39, *H. pratti*: 57, *R. ferrumequinum*: 36. 28

2.9 **Direction-dependent Doppler shift signatures received at the ear canal of a deforming biomimetic pinna.**

A) Spectrogram of an example Doppler signature (azimuth 60° , elevation 0°) with a superposed prediction of the maximum Doppler shift based on pinna surface velocity estimates (magenta line). The arrow indicates the start of the pinna motion. B) Maximum number of direction that could be distinguished based on Doppler signatures as a function of the signal-to-noise ratio. C) Clustering result showing an orderly break-up of the direction space based on the Doppler signatures. The different gray scale values and numbers denote the clusters that Doppler signatures for the respective direction were assigned to. 30

2.10 **Doppler signatures received as a function of different directions of sound incidence.**

The directions of the Doppler signatures shown ranged from -30° to 60° in azimuth and from -30° to 30° in elevation. The respective direction (azimuth,elevation) is indicated above each spectrogram. 31

3.1	Experimental setup: A) Biological inspiration from the Doppler shifts produced on the surface of a bat pinna (Pratt’s roundleaf bat, <i>Hipposideros pratti</i>). Doppler shift amplitudes were derived from the velocities of the pinna surface relative to the propagation direction of the incoming ultrasonic wave are color-coded on the pinna surface [1]. B) Biomimetic silicone pinna mounted on a pan-tilt unit used to orientate the setup for direction sampling and source tracking. The pinna is deformed by a servo motor via a cam and string attached at the pinna tip. C) electrostatic loudspeaker with a screen attached for quantifying the alignment of the pinna with the speaker. D) biomimetic pinna mounted on a pan-tilt-unit with a laser pointer to indicate the orientation of the pinna aperture.	38
3.2	Diagram of the CNN architecture: A) overall CNN architecture, B) filter set, C) convolution block. The number of different convolution kernels in each filter set is denoted by k	40
3.3	Doppler shift signatures associated with different directions: Normalized spectrograms of ultrasonic signals received from directions ranging over 90° in azimuth and 60° in elevation. The direction associated with each spectrogram is given as [azimuth, elevation] in the respective panel. The frequency axis of the spectrogram has been centered at the emitted frequency and hence directly gives the value of the Doppler shift.	43

3.4	Deep learning of direction finding from Doppler signatures: A) training and validation loss; B) prediction results. All errors (training, validation, and prediction) were quantified as a root-mean-square error. The averages for training (thick black solid line) and validation losses (thick gray solid line) were based on 20 repetitions of the learning process. The standard deviations in this sample are indicated by thin dashed black lines and thin gray lines respectively. After training, the prediction accuracy of the network was tested with 300 inputs. Prediction results are given for azimuth (main graph) and elevation (lower inset). To further characterize the variability of the estimates as a function of the true direction, fits of Gaussian distributions to the prediction values for three different true azimuth values (-45° , 0° , 45° , $N=21$, 23 , 23 respectively pooled from the five nearest directions).	44
3.5	Accuracy of direction finding with a dynamic soft-robotic pinna: The ability of the soft-robotic pinna mounted on a pan-tilt unit to track a sound source in azimuth was assessed in two different ways: (i) by virtue of the azimuth value that was predicted by the DNN (dashed line) and (ii) by the pointing direction of a laser pointed mounted on the pinna (solid line). Perfect predictions are indicated as a reference (dotted line). The soft-robotic pinna was presented with ultrasound signals from $N=61$ different directions in azimuth.	45
3.6	Direction-finding paradigms: A) single sensor with multiple frequencies, B) single frequency with multiple sensors, C) single frequency with a single dynamic sensor.	46

List of Abbreviations

\mathbf{K}_{nn}	The covariance matrices of the noise
\mathbf{K}_{yy}	The covariance matrices of the noise data
\mathbf{n}	A vector of Gaussian white noise
σ^2	The variance of the Gaussian white noise
2D	two-dimensional
3D	three-dimensional
cf	constant frequency, amplitude modulation
CNN	Convolutional Neural Network
dB	decibels
fm	frequency modulation
SNR	Signal-to-Noise Ratio
SOZ	signal overlap zone

Chapter 1

Introduction

1.1 Bat Biosonar System

Bats (order Chiroptera) are a group of animals that have achieved a remarkable evolution success and are known for their echolocation ability [2]. By emitting calls out to the surroundings and then receiving echoes that reflect from various targets nearby, bats can identify, locate, and characterize the targets in the darkness [3]. To date, up to 1,400 bat species have been documented [3], and they are traditionally categorized into two suborders: megabats and microbats. The former is largely fruit-eating, and the latter includes about 1,200 species that echolocate [4].

Biosonar is widely utilized for navigation, foraging, and hunting in different environments. Like other echolocating animals, such as birds [5], whales [6] and dolphins [7], bats have outstanding echolocation performance. They have developed a sophisticated biosonar system through the long evolution process of about 50 million years [8]. Bats send out sound waves that bounce off prey and potential obstacles to probe their surroundings [2, 3]. The ability to extract remarkably detailed information about their environment from biosonar signals allows bats to accomplish extraordinary sensing and navigation tasks.

Bats are the only mammals capable of genuine sustained flight, and they could do maneuvers such as tight turns, hovering, and perched landing in an upside-down manner [9]. They could

swoop close to the water surface and drink from it at fast speed [10]. Bats are social animals, and some species form large colonies up to a few millions of individuals [11, 12]. They can travel around 50 miles per night and always manage to get back to their home [13]. They could fly in swarms and manage to maneuver without crashing into each other based on some swarming mechanics like vocalization cessation [14], offensive jamming during feeding competition [15], leader-follower interactions [16] and pulse emission rates adjustment [17].

Bat calls range in frequency from 11 kHz [18] to 212 kHz [19]. The primary frequency of many insectivorous bats range from 20 kHz to 60 kHz [20], which extends beyond normal human hearing range (between 20 Hz and 20 kHz) [21]. These calls typically vary in intensity from 60 dB to 140 dB [22].

Big brown bat can hear a frequency of 1 kHz at its lowest and up to 120 kHz at its highest [23]. Bat calls can be categorized into four types: frequency modulated (FM), constant frequency (CF), or a combination of constant frequency / frequency modulation (CF/FM) or frequency modulation/constant frequency/frequency modulation (FM/CF/FM) pulses [24]. Different echolocation calls determine the type and quality of the information that contained in returning echoes. Bats developed different calls, for example in terms of frequency, duration, and intervals between pulses, to meet diverse sensory needs [25].

For instance, Horseshoe bats (rhinolophids, *Rhinolophidae*) and Old World leaf-nosed bats (hipposiderids, *Hipposideridae*) are two closely related bat families [26] noted for their sophisticated biosonar systems that share similar types of calls in frequency. Both bat species composite calls with CF and FM components to achieve target detection, classification, and locating [27]. The CF components promote detection [27] and classification [28] classification of insect prey by the Doppler shift caused by the insect wing beats and the final FM component enhances the positioning of the targets [29]. To detect the size of insect preys, horseshoe bats adapted the frequency of the emission in the process of evolution by exploiting

different harmonics in sets of harmonic bands [30].

Besides frequency, the duration and pulses intervals are the other two main features that well exploited by the bat biosonar system [25]. The duty cycle is a ratio of time that the signal is on compared to the time that signal is off. In the low-duty cycle echolocation, bats assign calls based on the estimate of the distance to the prey such that the returning echoes are separated. In the high-duty cycle echolocation, bats separate the emission and echo based on the information in frequency [25]. Bats are sensitive to a certain range of frequency. The receiving echoes contain Doppler shift caused by their flight and the Doppler shift reveals information relating to the location and motion of the prey. To keep echoes returning at the optimal frequency bands, bats adapted to adjust the frequency of the emitting pulse based on the flight speed [25]. The signal overlap zone (SOZ) was determined by the overlap between target echoes and the emitted call [31]. When bat approach targets, to avoid the overlap between pulse and echo, they usually reduce call duration to keep the SOZ not longer than the distance to the target [25]. To guarantee all echoes returning from the former pulses received before the next emission, bats flying in open spaces use longer pulses with longer intervals between pulses than those flying in clutter [25].

Bats actively modify the duration, direction, timing, intensity, and spectral content of their calls in response to information carried by the echoes, which allows them to flexibly react to changes in the environment [32], such as the trajectory of a target [33]. The big brown bat (*Eptesicus fuscus*) generates FM echolocation signals to hunt for flying insects [34]. When approaching the prey and start the target capture, bat increases the rate of the sonar calls and locks the sonar beam onto the target [35, 36]. Early experiments on the bat target tracking indicated that big brown bats use a non-predictive strategy (only using the information from the last returning echo) [37, 38], while recent evidence showed that bats also leverage a more sophisticated prediction model for moving target's trajectory by integrating signals over time

to achieve the prey capture under conditions of uncertainty [32]. When the prediction of the target trajectory is disrupted by a sudden target maneuver, the bat rapidly increases sonar scan frequency to recapture and update the internal state of the target trajectories to re-enable tracking of the escaping prey [32].

In fact, a new study has reported that bats have a very good sense of their surrounding environments, to the extent that they can perform large-scale environment mapping, and reason map-based navigation [39]. The binaural differences in return time, intensity, and echo spectrum encode the rich information on target location in terms of azimuth, elevation and distance [40, 41, 42, 43, 44, 45], which allow the bats to map environment and targets in a three-dimensional space. Some studies have examined the precision of such mapping capability: the acuity for the big brown bat to separate pairs of horizontal rods in the vertical plane was 3° [40], while the tracking accuracy of the same bat species in the horizontal plane is 1.6° [46].

Equipped with such intricate biosonar system, bats become the only mammals that are capable of (advanced) powered flight, such as complex maneuvers [9], commute long distances [13], fly fast & high [47]. Bats have developed a very unique flying system that differs from all other flying animals in wing structure and flying kinematics [48]. The size of the wingspans range from giant flying fox with 1.5 m to the tiny bumblebee bat with only 15 cm [49]. Unlike the more rigid wings of birds and insects, soft bat wings are much more pliable due to the extra degree of freedoms allowed by the flexible membrane and multiple joints [50]. Touch-sensitive receptors are distributed on the small bumps of the wing surface, enabling the bats to feel and adapt to the changing airflow while allowing the accurate execution of subtle maneuvers for in-flight prey capture [51].

1.2 Emitter and Receiver Dynamics of Bats

In echolocating bats, sophisticated motor dynamics are found in the emission and reception of sonar pulses [52]. Most echolocating bats emit sound through the mouth [53] or noseleaf [12]. Beamforming tests reported that mouth-emitting Bodenheimer’s pipistrelle bats (*Hypsugo bodenheimeri*) dynamically adjust their mouth gape to optimize the space that they sense in both natural field conditions and a controlled experimental environment [54]. Bat typically narrowed the beam when approaching a limited area and widened it within a few dozen milliseconds when entering an open area. [54].

Bat species send out ultrasound via the nostrils have a noseleaf to assist in forming the emission beam. [55]. Horseshoe bat, as an example, has highly evolved noseleaves that consist of three parts: anterior leaf, sella, and lancet [12]. Beyond the static geometrical complexity of the noseleaf and their shape features, the emitter also has a dynamic dimension [12]. Greater horseshoe bats move both anterior leaf and lancet during pulse emission [56, 57]. Similar acoustic dynamics in the emission beam was also reported for the Japanese horseshoe bat (*Rhinolophus ferrumequinum nippon*) [58].

The research found that the noseleaf can enhance the emission in the forward direction and also could narrow the beam width. [59]. In an experiment of the noseleaf bat of family Phyllostomidae (*Carollia perspicillata*), by bending the noseleaf lancet backward and fixed it to the bat’s forehead, researchers found that this approximately doubles the vertical range of the emission beam while keeping the horizontal spread unaffected, which indicated that the noseleaf played a role in target elevation determination [60]. The numerical studies [61, 62, 63] also suggested that noseleaf structures and changes affect the emission beam properties.

On the reception side, horseshoe bats have quite big outer ears (pinnae) (22 mm to 23 mm) compared to their head (20 mm) [64]. In the horseshoe bat, there are about 20 muscles

related to the pinna actions, with many of them are entirely located on the pinna [65] to allow the bat execute complex ear motions during biosonar behaviors [66, 67, 68].

Two types of pinna motions have been found for Horseshoe bats and Old World leaf-nosed bats: rigid and non-rigid [69]. The non-rigid motion causes substantial changes in the ear structure to compare to the rigid one [69]. Pinna motions in the horseshoe and hipposiderid bats could serve the animals' sensing in different ways: (i) a rigid component that reorients the beampattern [70], (ii) a non-rigid, linear component that changes the pinna's beampattern by the pinna geometry. The rigid component can be easily understood as a scanning operation where the most sensitive coverage of the beampattern is re-pointed in different directions. The non-rigid, linear motion components have been demonstrated to enhance the encoding of sensory information related to direction-finding [71].

Conspicuous pinna motions [67, 68, 72, 73, 74] are an integral part of biosonar behaviors in horseshoe bats and Old World leaf-nosed bats (families *Rhinolophidae* and *Hipposideridae*) [12, 75]. These motions have been reported to improve sensing and navigation performance [71, 76, 77], but the functional role of these dynamic features and the underlying mechanisms have yet to be fully understood [12]. Emitter or receiver motions can result in Doppler shifts, i.e., nonlinear scaling of signals in time and frequency in the acoustic domain [12]. Bats' own flight motions are sources of self-generated Doppler shifts that are regarded mostly as undesirable side-effects of the animals' mobility that need to be compensated for [78]. To date, prey-generated Doppler shifts are the only well-established solution to the problem of identifying prey in the clutter with active biosonar [79]. The possibility of pinna-induced Doppler shifts had been conjectured in the early work of Pye [67, 68, 80]. In general, horseshoe bat pinna motions are unlikely unintentional byproducts since the animals have actively seek to produce them, e.g., through an elaborate pinna musculature [72].

1.3 Experimental Study of Biosonar Dynamics in Bats

Evolution has shaped the powerful abilities of animals and as manufacturing materials, actuators, and controls developed, it is possible to mimic the natural world. Such aims, however, are restricted by the short of development of sophisticated actuators for biomimetic dynamics, and at a more fundamental level, by deep gaps in the understanding of the basic mechanics of the 3D complicity of animal motions [48]. So that learning the animal dynamics is not only contributing insight to the biological system but also could provide adequate thoughts to the engineered design.

Bat as the only flying mammals capable of sophisticated biosonar dynamics has been studied at spatial and temporal scales cover the motion of their emitter [57, 81, 82, 83, 84, 85] and receiver [69, 86, 87] to the maneuvering flight [48, 88, 89, 90, 91, 92]. Normally, the motions are captured by the high-speed video cameras, and then the recordings are digitized to provide a qualitative understanding of animal motion or quantitative analysis by the 3D reconstruction [90]. Software techniques for image processing and trajectories 3d reconstruction from multiple calibrated cameras with applications to the biological area were well-established. [93].

Extracting the positional information from video recordings includes two coupled problems: identifying the specific objects or landmarks from the video frames and reconstructing the identified object by mapping pixel coordinates from one or more cameras to 2D or 3D coordinates [93]. Landmarks usually are identified either by manually picking, which can be very time-consuming, or by software. A new learning technique (DeepLabCut) for 3D pose estimation by combining transfer learning and deep neural networks. enable to track features automatically with minimal training data (typically 50-200 frames). This technique has already been used for the study in both lab and wild animals, for example, pose es-

timation [94] and social behavior in bats [95]. After reconstructing the 3D trajectory of the landmarks, the velocity, acceleration, rotation angle, etc., could be calculated for further analysis. The well-established motion capture and information extraction system have enable the experimental measurements and analysis of the bat and its replications' ear [69, 86, 87] and noseleaf [57, 81, 82, 83, 84, 85] motions.

The high maneuverability and stability of bat flight have arisen rich research in flapping-wing flight mechanics. Research studies the kinematics of bat flight [96, 97, 98, 99, 100] to determine the fundamental kinematics. Experiments with around 20 reflective markers placed on the wing in straight and turning flight[48] completed under both the natural environment and in a wind tunnel at different speeds [101] show that dimensional complexity of the kinematics did not change with flight speed [101]. Except for the utilization of modern wind tunnel technology, the quantitative experimental study takes advantage of flow visualization techniques, like particle image velocimetry (PIV) [48, 91, 92], to measure the wake velocity structure in bat flight. To better understand the aerodynamics of bat flight, the flight trajectory estimation has been analyzed with a multi-view camera system [88, 89] and the detailed force measurements were computed via computational fluid dynamics analysis [48].

1.4 Bat-inspired Sensing Systems

Inspiration from biosystems has long been a popular drive for designing robots that walk, run, swim, or fly. The ultra efficiency, adaptability, maneuverability of biomechanics, refined by natural evolution, promises to improve the current robotics system [90]. Studies on the motion of humans [102], insects [103], snakes [104], bats [105], fish [106], etc., have served as a basis for robotic design. Bat capable of the sophisticated biosonar system and the complicated flight maneuvers, keep inspiring engineers to design different types of sensors

and robotics to understand and replicate the success of bat flying system.

To better understand how the shape-changing of the noseleaf and pinna influence the acoustic characteristics of the emission and reception, biomimetic systems such as robotic sonar heads based on horseshoe bats with actuated flexible baffles were developed. The latest version of the biomimetic pinna model achieved motor feedback based on the development of a soft actuation system along with a prototype strain sensor [107]. Sonar [108] and radar [109, 110, 111] are two well-known sensor techniques to the public, which have apparent parallels with bat biosonar where in both cases FM waveforms (“chirps”) are used for distance estimation and Doppler shifts are used for relative velocity inference [12, 25]. Inspired by bat’s capability to distinguish the different type of preys from the clutter-producing background vegetation, a mobile robot equipped with an acoustic sensor can accurately classify terrain types [112], as well as distinguish walls, fences, and hedges [113] based on the analysis of sonar echoes and machine learning techniques. Different biosonar behaviors in bat’s prey searching [114], target positioning [115, 116, 117, 118] and crowd swarming [119] in space, motivate the bat-inspired algorithm (a swarm-based intelligent system) implemented in the wireless sensor network. Such techniques are applied in various situations to carry out different tasks like search, rescue, disaster relief, target tracking in complex environments [115].

Inspired by nature, engineers have designed flying robots like insect-size [120] and bird-size [121] flapping robots that can be applied in surveillance and rescue missions [122]. Other than birds and insects, the bat maneuvers have also been extensively studied to generate new design principles for flapping-wing robots. In general, it is very difficult to study the aerial locomotion of bats due to the complex relationships between their morphology and flight capabilities [122]. The researcher built many different types of bat-inspired fly robotics in recent years to understand how bats manage their body posture and position by the intricate interactions of nonlinear aerodynamic forces and their musculoskeletal control [122]. An early

attempt of a bat-inspired flapping-flight platform was designed and built with shape memory alloy muscles and joints [123]. To study the relationship between kinematics, power input, and aerodynamic output, a multi-articulated bat-wing was constructed to measure power input and force output simultaneously that across a range of kinematic parameters [124]. The researcher also developed a miniature integrated jumping and gliding robot, the “MultiMo-Bat”, to mimic the locomotion strategy of vampire bats [125]. More recently, a biologically inspired soft robot called Bat Bot (B2), a flapping machine with five degrees of actuation, was developed [122] based on the previous work [124, 126] studying bats’ physiology and flight specializations.

Chapter 2

Discoveries in the Bat's Biosonar System

2.1 Title

Fast-moving Bat Ears Create Informative Doppler Shifts

2.2 Abstract

Many animals have evolved adept sensory systems that enable dexterous mobility in complex environments. Echolocating bats hunting in dense vegetation represent an extreme case of this where all necessary information about the environment must pass through a parsimonious channel of pulsed, one-dimensional echo signals. We have investigated whether certain bats (rhinolophids and hipposiderids) actively create Doppler shifts with their pinnae to encode additional sensory information. Our results show that the bats' active pinna motions are a source of Doppler shifts that have all attributes required for a functional relevance: (i) The Doppler shifts produced were several times larger than the reported perception threshold; (ii) the motions of the fastest moving pinna portions were oriented to maximize the, Doppler shifts for echoes returning from the emission direction indicating a possible evolu-

tionary optimization; (iii) pinna motions coincided with echo reception; (iv) Doppler-shifted signals from the fast-moving pinna portion entered the ear canal of a biomimetic pinna model; (v) the time-frequency Doppler shift signatures were found to encode target direction in an orderly fashion. These results indicate that instead of avoiding or suppressing all self-produced Doppler shifts, rhinolophid and hipposiderid bats actively create Doppler shifts with their own pinnae. These bats could hence make use of a previously unknown nonlinear mechanism for the encoding of sensory information that based on Doppler signatures. Such a mechanism could be a source for the discovery of sensing principles that would not only be new to sensory physiology but could also to the engineering of sensory systems.

2.3 Introduction

Conspicuous pinna motions [67, 68, 72, 73, 74] are an integral part of biosonar behaviors in horseshoe bats and Old World leaf-nosed bats (families Rhinolophidae and Hipposideridae, [12, 75]). These motions have been demonstrated to enhance sensing and navigation performance [71, 76, 77], but the functional role of these dynamic features and the underlying mechanisms have yet to be fully understood [12]. In the acoustic domain, source or receiver motions can result in Doppler shifts, i.e., nonlinear scaling of signals in time and frequency. The possibility of pinna-induced Doppler shifts had been mentioned as an aside in early work by Pye [67, 68, 80], but has not been considered further – let alone investigated in any depth – in the literature since. This complete neglect is regrettable, because ear-generated Doppler shifts could constitute a previously unknown, nonlinear mechanism for the active encoding of sensory information. To test this hypothesis, we have carried out a quantitative experimental investigation of the hypothesis that pinna motions cause functionally-relevant Doppler shifts in bats. For pinna-generated Doppler shifts to have a

functional role, five necessary conditions must be met: (i) pinna surface speeds must be high enough to produce Doppler shifts that exceed the animal’s perception threshold (here we use the ~ 50 Hz standard deviation of Doppler shift compensation, [127, 128, 129, 130]), (ii) the directions of pinna surface velocity and echo propagation must be aligned well enough to translate the surface speeds into sufficiently large Doppler shifts, (iii) fast pinna motions must occur during echo reception, (iv) Doppler-shifted waves from the fast moving portions of the pinna surface must enter the ear canal, and (v) the Doppler signatures must convey useful sensory information.

2.4 Materials and Methods

2.4.1 Overall Experimental Setup and Animal Care

During the experiments, each bat was placed on a platform consisting of a piece of planar wire-mesh grid that was rotated 45° relative to the horizontal so that the bat’s head was lower than its feet when positioned on the platform. On this platform, the bat was positioned in the center of the setup (Fig. 2.1B) and at a distance of 50 cm from the microphones in the array that was used to record the ultrasound and 55 cm from the high-speed video cameras that were used to record the pinna motions. All potential sound-reflecting surfaces in the setup were clad in sound-absorbing foam during the experiment.

Two adult greater horseshoe bats (*Rhinolophus ferrumequinum*) were taken from a cave near Jinan, Shandong province and five hipposiderid bats, two greater Himalayan roundleaf bats (*Hipposideros armiger*) and three Pratt’s roundleaf bats (*Hipposideros pratti*) were taken from caves in two different regions in southern China, in the vicinity of Sanming city, Fujian province, and Suiyang city, Guizhou province.

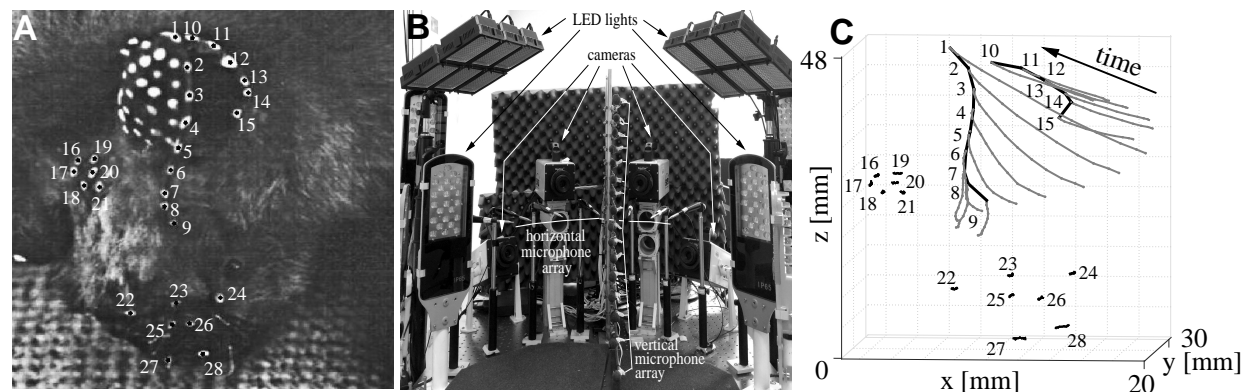


Figure 2.1: **Experimental setup for the animal experiments.** A) example high-speed video frame showing the landmark points placed on the pinna rim (point numbers 1 to 15), noseleaf (point numbers 22 to 28), and head (point numbers 16 to 21) of a hipposiderid bat to facilitate motion capture B) setup consisting of an array of four high-speed video cameras, LED illumination from two directions, and an array of seven measurement microphones. High-speed cameras and microphone data acquisition were synchronized. C) 3D reconstructions of the motion trajectories of the points shown in (A). The arrow indicates the motion direction with time. The rim of the pinna and the end point of the motion shown on panel A).

The bats were kept in indoor flight rooms (each 1.3 m wide, 6 m long, and 3 m high) separated by genus. The rooms provided a controlled environment with constant temperature (23°C) and humidity (60%). In order to ensure that the bats were active during the times of the experiments, the day- and nighttime of animals were switched in the flight rooms. The daily light-dark cycle in the rooms consisted of 10 hours light and 14 hours darkness. The bats were fed a daily diet of mealworms enriched with vitamins and mineral supplements and were provided water *adlibitum*.

2.4.2 3D Reconstruction of Pinna Motions

Quantitative characterizations of the pinna motion kinematics were obtained based on three-dimensional reconstructions of the time-trajectories (Fig. 2.1C) belonging to discrete landmark points that were placed on the pinna (Fig. 2.1A). The landmark points were placed on

the bats using a nontoxic dye before the experiments and removed (washed off) immediately after the end of each experiment. For each experiment, approximately 60 different landmark points were distributed over the pinna surface with an emphasis on coverage of the pinna rim. Five to seven additional landmark points each were placed on the top of the head and the noseleaf of the animal to provide an anatomical frame of reference for the pinna motions.

Video image sequences with views of the bats' heads, their pinnae, and the associated landmarks were captured using an array of four high-speed video cameras (GigaView; Southern Vision Systems, Huntsville, AL, USA) with 50 mm lenses (Rodagon, Rodenstock, Feldkirchen, Germany). All cameras were operated with a frame rate of 400 Hz and a digital image resolution of 1280×1024 pixels. The high-speed cameras were calibrated to obtain estimates of their internal and external parameters based on calibration images taken of a checkerboard pattern from different viewing directions [131]. The image coordinates of each landmark point were obtained using video frames from at least two different high-speed video cameras that had imaged the landmark of interest at the respective time. The image locations of the landmark were picked manually in the rectified video frames. The high-speed video cameras to be included in the stereo reconstruction were selected manually based on how well their images had captured the landmark points during a given motion. Finally, the image coordinates were used to reconstruct the three-dimensional location of the landmark points using stereo triangulation [131].

2.4.3 Ultrasound Recording

A capacitive measurement microphone (1/8" pressure-field microphone, type 40 DP, with type AL0003 preamplifier, G.R.A.S. Sound & Vibration, Holte, Denmark) was used to record the echo returns at the position of the bats. The microphone was placed approximately one

centimeter above the bat's head. The microphone was calibrated with a sound level calibrator (type 4231, Brüel & Kjær, Nærum, Denmark) at 114 dB SPL and a frequency of 1 kHz. The output signals of the microphone were digitized with a sampling rate of 512 kHz and 16 bits resolution (common-mode rejection ratio 75 dB, PXIe-6358 data acquisition board, National Instruments, Austin, TX, USA). Additional microphones (measurement microphones, type 40 DP, G.R.A.S. and capacitive MEMS microphones, Momimic, Dodotronic, Rome, Italy) were placed in a vertical and a horizontal line array to record the emissions of the bats in the setup. The microphones and the high-speed video cameras were triggered simultaneously using a custom LabVIEW control software. The control system produced a constant time offset of 16 ms between video and audio recordings that was compensated for during data analysis.

2.4.4 Biomimetic Pinna Experiments

A biomimetic pinna shape was designed based on the μ CT scan of an adult horseshoe bat pinna specimen. The shape was simplified by eliminating small geometric detail in the digital domain (Autodesk Maya [132]) while keeping the overall shape of the original. The simplified design was used to create a rigid physical model of the pinna shape with additive manufacturing. This rigid physical model was used to create a mold and then cast a flexible biomimetic pinna in silicone (Ecoflex, Smooth-On, Inc., Macungie, PA, USA) (Fig. 2.2A). The biomimetic pinna designed and fabricated in this way had a height of 5.8 cm, i.e., about twice the size of the pinna in greater horseshoe bats. An electrostatic loudspeaker (Series 600 open face ultrasonic transducer, SensComp, Livonia, MI, USA) was used to emit ultrasonic pulses with a constant carrier frequency of 90 kHz (resting cf-frequencies in greater horseshoe bats have been reported to fall slightly above 80 kHz [12], but can exceed 100 kHz in other species of the genus [133]) and a duration of 150 ms (in greater horseshoe bats, pulse durations

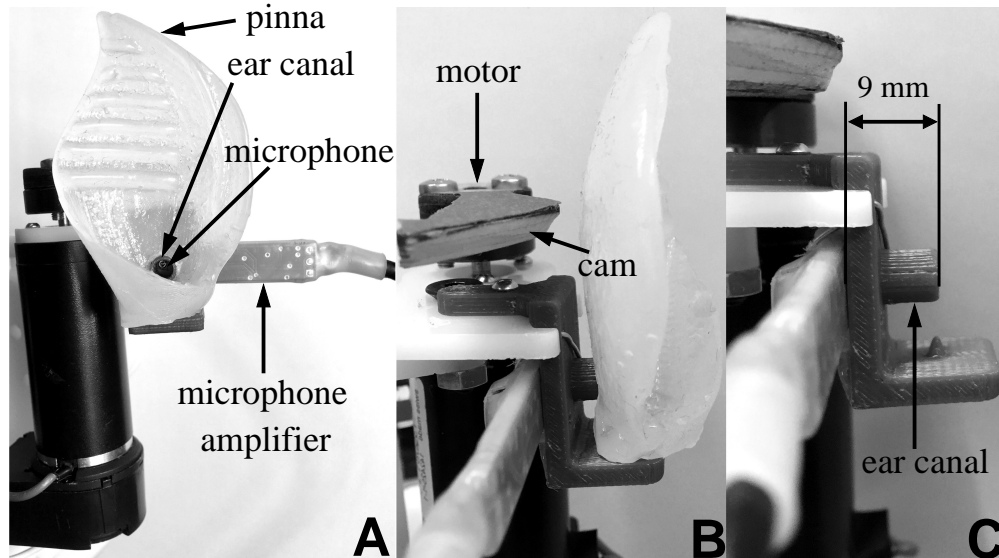


Figure 2.2: **Biomimetic pinna.** A) overview of the device, B) motor and cam shaft, C) pinna holder with the artificial ear canal.

up to 60 ms have been reported [134]). The parameters of the biomimetic pinna experiments were chosen for greater ease of experimentation without creating any differences that could affect the applicability of the results to the question whether pinna motions in the bats could create Doppler shifted signal components that enter the ear canal. The signal length was chosen so that the Doppler shift signature of a full forward and backwards pinna motion cycle could be recorded.

The signals mimicking the “echoes” impinging on the biomimetic pinna were emitted by a loudspeaker that was positioned at a distance of 50 cm in front of the biomimetic pinna. A capacitive MEMS microphone (Momimic, Dodotronic, Rome, Italy) was coupled to the pinna via an artificial ear canal (length 9 mm, diameter 4 mm) to record the received ultrasonic signals (Fig. 2.2C). The output of the microphone was digitized with a sampling frequency of 500 kHz and a resolution of 16 bits (PXIe-6356 data acquisition board, National Instruments, Austin, TX, USA). The 3d trajectory of the tip point of bat’s moving ear was reconstructed based on the video frames recorded with two synchronized GoPro HERO3+ cameras (Dual

HERO System, GoPro, San Mateo, CA, USA) at a frame rate of 120 Hz.

For recording direction-dependent Doppler signatures, the biomimetic pinna assembly (Fig. 2.2A) was mounted on a pan-tilt unit (model PTU-46-17.5, FLIR Systems, Inc., Burlington, ON, Canada). The pinna was rotated over a range of 180° in azimuth and 60° in elevation centered on the front facing direction of the pinna aperture in steps of 3° . Hence there were 61 different azimuth and 21 different elevation values, resulting in a total of 1,281 different directions that were surveyed in these experiments. For each of these directions, narrow-band ultrasonic pulses were emitted at the biomimetic pinna as described above. During each of the 150-millisecond recordings, the biomimetic pinna was held static for 20 ms and was in motion for the remaining 130 ms. For each of the motions, an estimate of the maximum Doppler shift was obtained from speed estimates for a landmark point that was placed on the pinna tip.

2.4.5 Data Sets and Processing

Pinna motion speeds: A total of 30 pinna motion sequences were analyzed for each of the three species studied. These sequences came from a total of seven different individuals. The individuals and analyzed sequences were distributed as follows: *Hipposideros armiger*: two individuals with 5 and 25 sequences each, *Hipposideros pratti*: three individuals with 2, 9, and 19 sequences each; *Rhinolophus ferrumequinum*: two individuals with 12 and 18 sequences each. For each of these motion sequences, the 3d trajectories (Fig. 2.1C) of landmark points placed near the pinna tip were reconstructed as a basis for estimating the motion speeds.

Angle between directions of pinna surface motion and sound radiation: To investigate the angle between the direction of the pinna surface velocity and the direction of sound radiation, 3d motion trajectories were estimated for 39 points distributed approximately

uniformly over the ear surface. For this experiment, 10 video frames representing a single pinna motion sequence obtained from a *Hipposideros pratti* individual were analyzed. The point in time when most landmark points had a high speed, i.e., close to maximum speed, was picked to show the ear motion direction and the normal of the noseleaf fitting plane was used as the pulse direction. To visualize the distribution of speed, angle, and Doppler shift over the inner surface of the pinna, a two-dimensional Gaussian was used as a radial basis function kernel to interpolate the values of these variables over the entire ear surface based on the measurements taken from the 39 landmark points.

Time relationship between pinna motions and echoes: A total of 132 sequences of synchronized high-speed video and ultrasound recordings were analyzed to investigate time relationship between pinna motions and the echoes. These sequences were distributed as follows: *Hipposideros armiger*: 39 sequences from 2 individuals, *Hipposideros pratti*: 57 sequences from 3 individuals, *Rhinolophus ferrumequinum*: 36 sequences from 2 individuals. From these sequences, a total of 132 echoes were analyzed.

Biomimetic pinna experiments: For each of the two experimental conditions, moving pinna and static pinna, 30 ultrasound recordings (duration 35 ms for each recording, sampling rate 500 kHz) were obtained. The ultrasound recordings were transformed into the frequency domain using a discrete Fourier transform with a 17,500-point Hamming window spanning the entire signal duration. The 30 repetitions among the recordings were used to estimate the average and the standard deviation of the spectrum. The spectrum estimates show a clear spectral broadening for the pinna motion condition when compared to the static condition (Fig. 2.3) validating the presence of pinna-motion-induced Doppler shifts in the ultrasonic signals entering the ear canal of the biomimetic pinna.

In order to compare the time course of the pinna motion to that of the spectral composition of the recorded ultrasonic signals, a spectrogram representation of the ultrasound signals

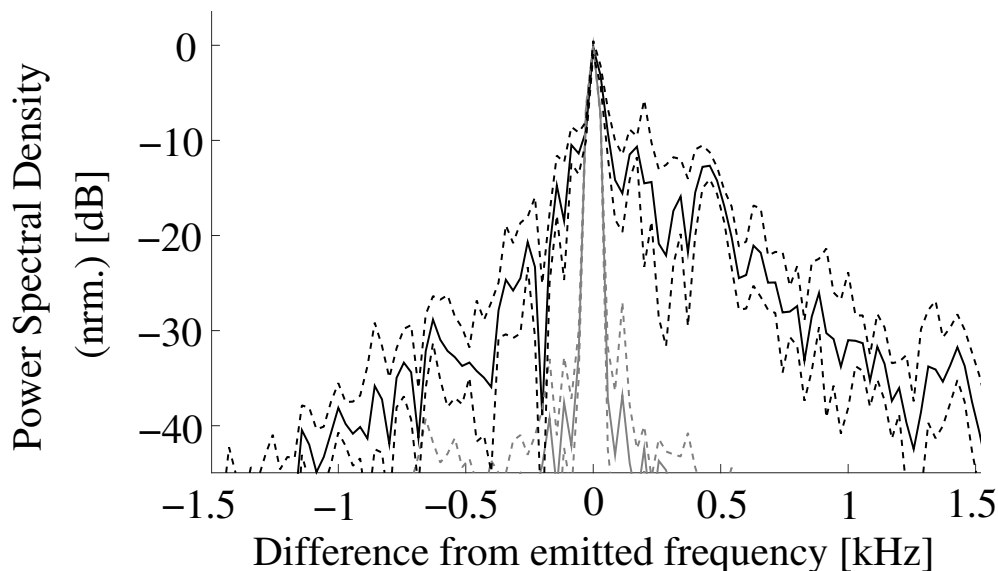


Figure 2.3: **Doppler shifts received at the ear canal of biomimetic pinna.** Power spectral density of the signal received in ear canal with (black lines) and without (gray lines) ear motions. Dashed lines show the standard deviations of the spectrum estimates ($N = 15$ for each condition).

was computed using a short-time Fourier transform with a 6000-point Hanning window and 50% overlap. The results (example in Fig. 2.9A) show that the estimates for pinna surface speeds are good predictors for the largest Doppler-shift magnitudes observed in the respective spectrogram.

To obtain Doppler signatures from the ultrasound recordings, spectrograms were computed using a short-time Fourier transform with a 6000-point Hanning window and 50% overlap. The power spectral density values of each of these spectrograms were normalized by their respective maximum over all times and frequencies.

Clustering of Doppler signatures: For clustering of the Doppler signatures, the spectrogram representations of the Doppler signatures were subsampled in the time as well as in the frequency domain. Subsampling in time used 35 points that were equally spaced along the signatures' duration. In the frequency domain, 25 point were equally spaced over the

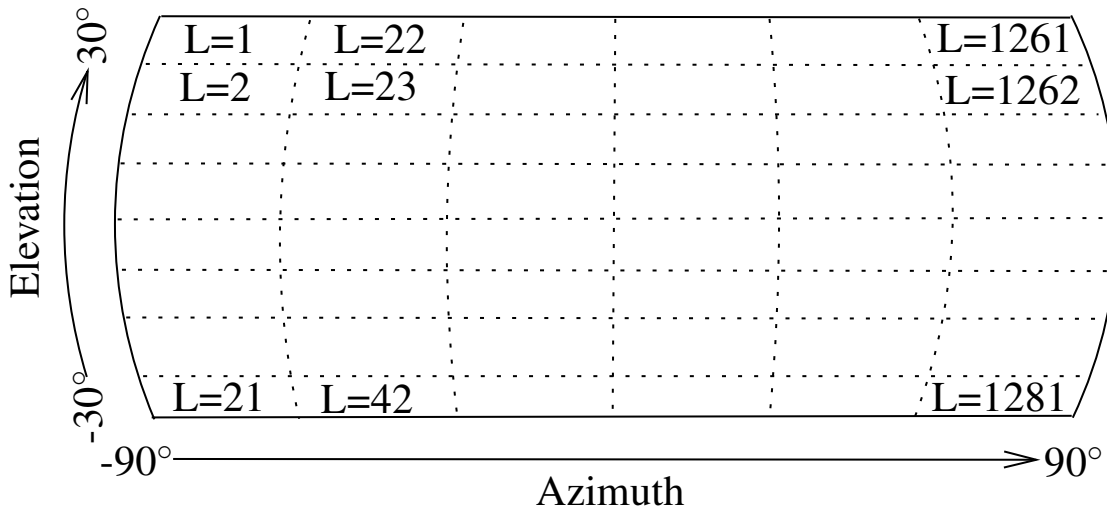


Figure 2.4: **Information-theoretic paradigm for finding an upper bound on the number of resolvable directions for biosonar targets:** The method assumes that the direction (azimuth and elevation) space is divided into resolvable sub-regions. The estimate on the maximum number of resolvable regions does not make an assumption on the size and shape of the regions, hence they may not be uniform as depicted in the sketch shown here.

frequency band that ranged between Doppler shifts of minus and plus 1 kHz. The data matrices representing these subsampled spectrograms were rearranged into feature vectors (of length 875) that contained all power spectral density values of the resampled spectrograms.

The vector representation of the subsampled spectrograms were used to cluster the measured Doppler signatures using a spectral clustering approach [135] based on a normalized algorithm [136] was used (Matlab implementation by I. Bürk [137]). The input data for the clustering was a matrix containing 1281 data points (i.e., Doppler signatures), each with 875 dimensions (spectrum amplitudes over time and frequency). The number of clusters was fixed at 50.

Upper bound on number of resolvable directions: An upper bound on the number of directions that could be distinguished based on the associated Doppler signatures was estimated by virtue of on an information-theoretic paradigm that treats direction-finding as a communication problem (20).

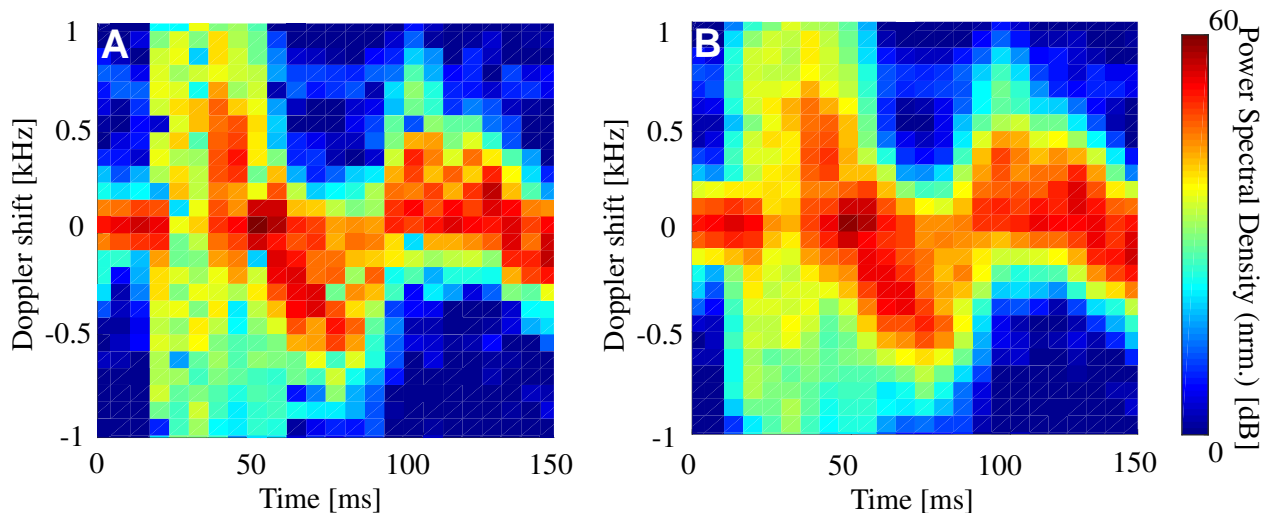


Figure 2.5: **Doppler signatures created by ear motion.** A) example of raw spectrogram, B) smoothed spectrogram (2-D Gaussian image filter with a mask size of 3 pixels and a standard deviation of 0.5 pixels).

The approach assumes that the space of all possible directions that the biosonar target could be located at is divided into a grid of cells that can be labelled $L = 1, 2, \dots, N$ cells (Fig. 2.4, where N is assumed to be 1,281). To match the experiments with the biomimetic sonar head, the biosonar target could be located anywhere in the region of this direction space that falls within the interval $[-90^\circ, 90^\circ]$ for the azimuth value and the interval $[-30^\circ, 30^\circ]$ for the elevation value. If this region of the direction space is covered by 1,281 cells, for example, and all cells are equally likely, the target direction will take at most $\log_2(1281) \approx 10.3$ bits to describe by virtue of these cells. The problem of finding the direction of a biosonar target can be thought of as communication problem in which the target transmits a message through the echoes. The content of this message is which grid cell contained the target and the message is received by the ear. The objective for the direction finding algorithm is to minimize the probability of choosing an incorrect grid cell for the target direction based on this message.

The method is based on a Gaussian channel model and the mutual information between the

source location and the (noisy) observations. It has been previously applied to the problem of encoding target-direction information by changing pinna shapes (9). To carry out this analysis on the Doppler signatures, the downsampled spectrograms (35 points in time and 25 points in frequency, s. above) were used. To avoid overestimates of the maximum number of discernible directions due to high spatial frequency content in the spectrogram images that may not represent reproducible features of the signatures, the spectrograms were smoothed by a 2-d Gaussian smoothing kernel (Fig. 2.5) (filter size 3 pixels, standard deviation 0.5 pixels). The spectrogram data was further compressed using principal component analysis (PCA). With this compression, the spectrogram data vectors were shortened in length from 875 to 13. These retained 13 eigenvectors accounted for 80% of the variability in the spectrogram data prior to this compression.

Under the Gaussian channel assumption, an upper bound on channel capacity (C , in bits) can be computed as (20):

$$C \leq I_{max}(\mathbf{x}, \mathbf{y}) = \frac{1}{2} \log_2 \frac{|\mathbf{K}_{yy}|}{|\mathbf{K}_{nn}|}, \quad (2.1)$$

where \mathbf{x} represents the Doppler signatures associated with a given direction, \mathbf{y} the noisy observations of these Doppler signatures, i.e., $\mathbf{y} = \mathbf{x} + \mathbf{n}$, where \mathbf{n} is a vector of Gaussian white noise with variance σ^2 . The matrices \mathbf{K}_{yy} and \mathbf{K}_{nn} are the covariance matrices of the observations and the additive noise respectively. The covariance matrices, e.g., for \mathbf{x} are given by:

$$\mathbf{K}_{xx} = E[(\mathbf{x} - E(\mathbf{x}))(\mathbf{x} - E(\mathbf{x}))^T]. \quad (2.2)$$

Finally, the signal-to-noise ratio (SNR) is related to the covariance matrix as

$$\text{SNR} = 10 \log_{10} \frac{\text{trace}(\mathbf{K}_{\mathbf{xx}})}{\text{trace}(\mathbf{K}_{\mathbf{nn}})} \quad (2.3)$$

The directional resolution enabled by the Doppler signatures can be expressed by the upper bound on channel capacity (C) or alternatively as the corresponding maximum number of distinguishable directions (given by 2^C).

To characterize the relationship between directional resolution and SNR, estimates for C were obtained for SNR values ranging from 0 to 16 dB.

2.5 Results

2.5.1 Fast Pinna Motion Speed

Using reconstructed 3d trajectories of landmark points placed on the pinna tips of individuals from three species with fast pinna motions (greater horseshoe bat, *Rhinolophus ferrumequinum*, and two hipposiderid species, *Hipposideros armiger* and *Hipposideros pratti*, Fig. 2.6), motion speeds up to ~ 2.2 m/s were found (Fig. 2.6A). While the ranges of the speed values overlapped among all species, there were statistically significant differences between them (Tukey’s range test, $p < 0.0001$ for all differences). Since all three species share a constant-frequency - frequency-modulated (cf-fm) biosonar system [19, 138], we have used the cf-component of the strongest (second) harmonic of the animals’ biosonar pulses [139, 140] for estimating the Doppler shifts corresponding to the tip speeds. Maximum Doppler shifts were calculated under the assumption that the direction of the maximum pinna surface velocity is aligned with the radiation direction of the echoes. The highest Doppler shift determined in this way was 383 Hz (for *H. pratti*, Fig. 2.6B). For the Doppler shifts, the difference be-

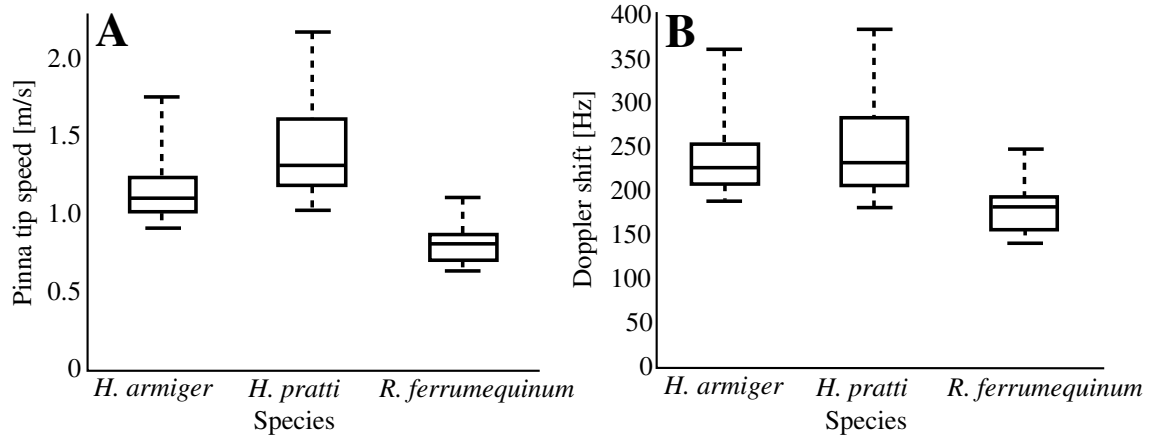


Figure 2.6: **Pinna tip speeds and maximum Doppler shifts for all three bat species studied.** A) Pinna tip speeds calculated from reconstructed 3d trajectories of landmarks placed on the pinna tip. B) Maximum Doppler shifts calculated under the assumption that the pinna moves in the direction of sound propagation (center line: median, box edges: 25th and 75th percentiles, whiskers: minimum and maximum values). Maximum Doppler shifts were calculated under the assumption that the direction of the maximum pinna surface velocity is aligned with the radiation direction of the echoes.

tween the two hipposiderid species was no longer significant ($p=0.47$), but the difference between the hipposiderids and the horseshoe bats remained significant (with $p < 0.0001$). The greater similarity in the Doppler shifts among the hipposiderids was due to the higher speeds occurring in the species with the lower cf-frequency (*H. pratti*, cf at ~ 60 kHz vs. ~ 70 kHz in *H. armiger*). Hence, it could be hypothesized that the pinna motion speeds in these hipposiderid species are adapted to produce similar Doppler shifts regardless of carrier frequency.

2.5.2 Direction Between Motion and Echo

Doppler shifts do not only depend on the speeds involved, but also on how the velocity vectors of these motions are oriented with respect to propagation vectors of the incoming echoes. The maximum Doppler shifts for a given speed are only realized if the velocity

vectors are parallel to the direction of sound propagation. We have used dense sampling of the pinna surface with landmark points to reconstruct the distribution of speeds and velocity vectors across most of the inner pinna surface. Based on ultrasonic array recordings done in the same experiments as the pinna surface velocity measurement, we have determined the direction in which most pulse energy was emitted as an estimate for where the bats were directing their biosonar beams and presumably were expecting the echoes to return from. We found that the highest speeds occurred in a region along the outer pinna rim that was a good match for where the orientations of the velocity vectors at maximum speed were close to parallel to the direction of sound radiation (Fig. 2.7). This spatial coincidence between high surface speeds and small angles between motion and sound radiation vectors could be hypothesized to be an adaptation that maximizes the Doppler shifts resulting from the pinna motions.

2.5.3 Motion Occur During Echo

For any potential impact on echo perception, the fast pinna motions must occur during echo reception. In order to assess whether this is the case, we have analyzed pinna motion speeds during echo returns with synchronized arrays of high-speed cameras and ultrasonic microphones. This data contained only pulse-echo sequences that were accompanied by fast pinna motions. We found that all echoes in these sequences coincided with Doppler shifts that exceeded the 50 Hz-accuracy reported for Doppler-shift compensation [127]. Depending on species, between 33% and 82% of the echoes coincided with pinna motions fast enough to produce Doppler shifts that exceeded this threshold three times (Fig. 2.8). Hence, this data suggests that all echoes in echolocation sequences accompanied by pinna motions contain Doppler-shift signatures that should be perceivable by the bats.

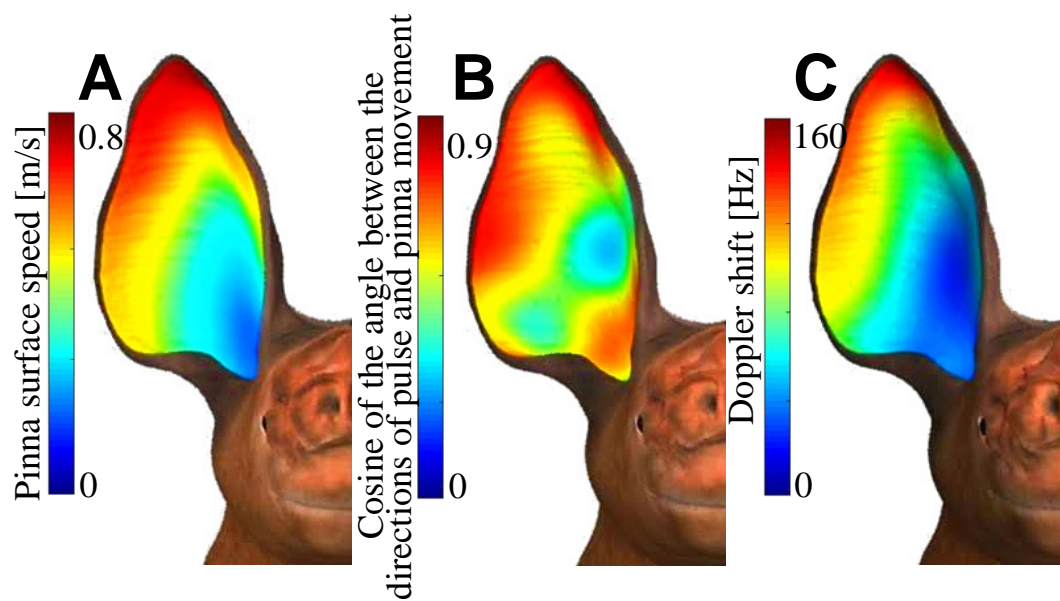


Figure 2.7: **Distribution of speed, directional cosine between surface velocity and radiation direction, and Doppler shift on the inner surface of the pinna.** A) maximum surface speed during a pinna motion, B) directional cosine between surface velocity and the direction of sound propagation associated with the maximum speed, C) Doppler shift estimates based on A) and B). Directional cosines were calculated under the assumption that the propagation direction of the echo corresponds to the direction associated with the maximum amplitude of the pulse.

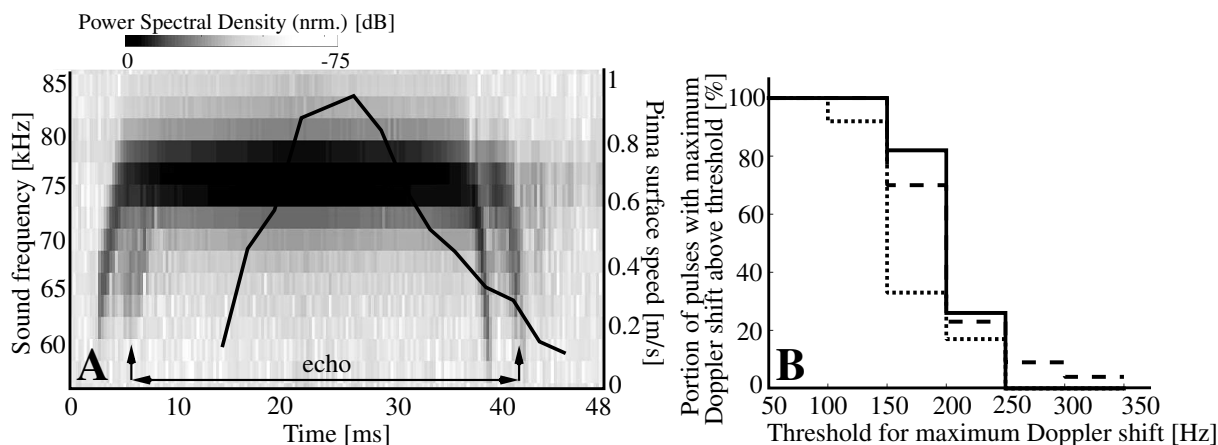


Figure 2.8: **Fast pinna motions and large Doppler shifts occur during echoes.** A) Pinna surface speed calculated from the landmark on the tip of the pinna superimposed on the spectrogram of biosonar pulse from RF and its echoes. In shown example recording, the pulses coincided with a forward motion of the pinna (positive speeds). B) Portion of pulses with maximum Doppler shift exceeding a certain threshold. Number of motion sequences/echoes analyzed: *H. armiger*: 39, *H. pratti*: 57, *R. ferrumequinum*: 36.

2.5.4 Doppler Shift From Recording and Calculation are Matching

Since only certain regions of the pinna surface (near the outer rim) move at speeds that are sufficiently large for the creation of perceivable Doppler shifts, we have investigated whether signal components diffracted by these regions enter the ear canal and could hence be perceived by the animals and supply useful sensory information. These experiments were based on a biomimetic pinna with a static geometry and deformation patterns that were qualitatively similar to the bats' pinna. We found that the biomimetic pinna motions produced strong Doppler signatures in the ultrasonic signals received inside the ear canal (Fig. 2.9A). As could be expected from the continuous distributions of speed over the pinna surface, the acoustic effects of the pinna motions took the form of spectral broadenings. We found the pinna tip velocity to be a useful predictor of the maximum Doppler shift (Fig. 2.9A). The sign of the observed Doppler shifts depended on the direction of the pinna motions. Since the bat species studied here exhibit alternating ear motions with one ear

moving forward while the other moves backward [67], the spectral spread of a combined binaural input could be about twice that produced by a single ear at any given time.

2.5.5 Doppler Shift Patterns

Finally, we found that the time-frequency Doppler signatures were direction-dependent (Fig. 2.9) and could hence be used to obtain information on the direction of a biosonar target. To quantify the available information, we have used an information-theoretic paradigm [141] that puts an upper bound on the number of directions that could be resolved as a function of the available signal-to-noise ratio (Fig. 2.9B). The results indicate that the Doppler signatures would be suitable to distinguish a large number of different target directions - even at fairly low signal-to-noise ratios, e.g., at a signal-to-noise ratio of 12 dB, up to about one million different directions could be theoretically distinguished. Furthermore, the Doppler signatures varied with direction in a systematic fashion. This was evident from the results of clustering the Doppler signatures based on their spectrogram representation yielded contiguous partitions of the direction space (Fig. 2.9C). This should help exploiting the direction-dependence of the Doppler signatures (Fig. 2.10) since small errors in estimating the Doppler shifts should result in likewise small errors in the direction estimates.

2.6 Discussion

All Doppler shifts that occur in bat biosonar can be classified as either prey-generated or self-generated. At present, prey-generated Doppler shifts are the only well-established solution to the problem of identifying prey in clutter with active biosonar [79]. The importance of prey-generated Doppler shifts is evident from numerous, far-reaching adaptations in bats

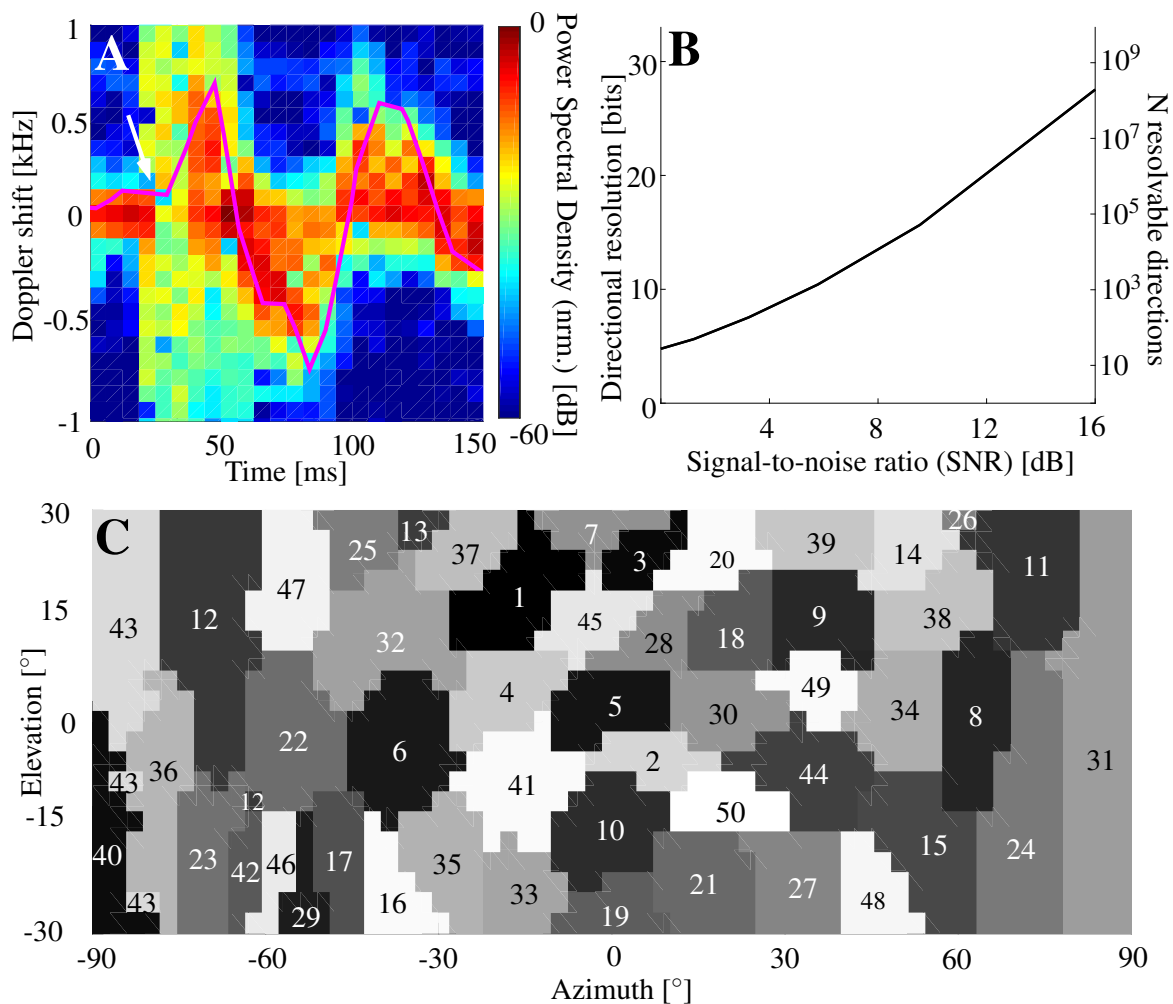


Figure 2.9: **Direction-dependent Doppler shift signatures received at the ear canal of a deforming biomimetic pinna.** A) Spectrogram of an example Doppler signature (azimuth 60° , elevation 0°) with a superposed prediction of the maximum Doppler shift based on pinna surface velocity estimates (magenta line). The arrow indicates the start of the pinna motion. B) Maximum number of direction that could be distinguished based on Doppler signatures as a function of the signal-to-noise ratio. C) Clustering result showing an orderly break-up of the direction space based on the Doppler signatures. The different gray scale values and numbers denote the clusters that Doppler signatures for the respective direction were assigned to.

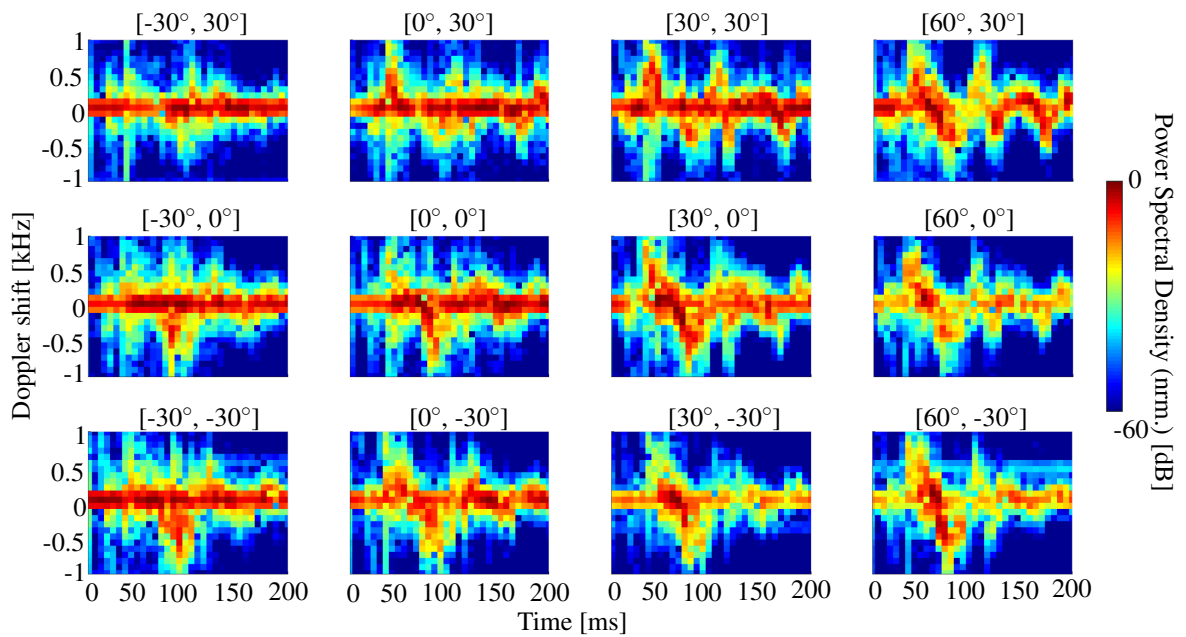


Figure 2.10: **Doppler signatures received as a function of different directions of sound incidence.** The directions of the Doppler signatures shown ranged from -30° to 60° in azimuth and from -30° to 30° in elevation. The respective direction (azimuth,elevation) is indicated above each spectrogram.

that range from pulse design to behavior and from the inner ear [142] to the auditory cortex [143, 144]. As of now, only the bats' own flight motions have been considered as sources of self-generated Doppler shifts. The resulting Doppler shifts have been regarded mostly as undesirable side-effects of the animals' mobility that need to be compensated for [78]. The possibility of flight-induced Doppler shift conveying information to support navigation has only been investigated using computational methods so far [145] and there is no published experimental evidence that bats make use of flight-induced Doppler shifts. Fast pinna motions constitute a previously unknown second source of self-generated Doppler shifts. In general, horseshoe bat pinna motions are unlikely byproducts since the animals seem to go such a great length to actively produce them, e.g., through an elaborate pinna musculature [72]. Furthermore, it has been reported that surgical disruptions of the pinna mobility have led to performance deficits in horseshoe bats [72, 76]. Similarly, the match between the regions of highest pinna surface speeds and the best alignment of the motion and sound propagation directions found here could be seen to argue in favor of functional significance of the Doppler shift to which the system has been evolutionarily adapted. However, much more data covering a larger number of species would be needed to test this hypothesis thoroughly.

Taking into account our current results, pinna motions in horseshoe and hipposiderid bats could serve the animals' sensing in three different, but non-exclusive ways, i.e., through: (i) a rigid component that reorients the beampattern [70], (ii) a non-rigid, linear component that changes the pinna's beampattern by virtue of the pinna geometry, and (iii) a non-linear, Doppler-based component. The rigid component is shared by many animals (e.g., head motions in humans) as well as technical sonar and radar systems. It can be readily understood as a scanning operation where the most sensitive region of the beampattern is moved into different directions. The non-rigid, linear motion components have recently been demonstrated to enhance the encoding of sensory information related to direction-

finding [71]. Changing the pinna geometry to produce a different beampattern shape can be seen as an alternative to change the frequency for a fixed pinna geometry [146]. The non-linear transformations due to the pinna-generated Doppler shifts described here add an additional quality to the pinna motions in bats. It remains to be determined if the Doppler-transformations of the echoes serve a functional purpose in the animals. If they are an integral part of the peripheral dynamics of the bats' biosonar system as the evidence presented here suggests, this would mean that the bats are able to harness non-linear effects that could lead to new functional principles for enhance sensing of natural environments and enable engineered sensory systems with the same capabilities.

Chapter 3

Applications of the Soft Robotics

3.1 Title

Integration of Deep Learning and Soft Robotics for a Biomimetic Nonlinear Sensing Paradigm

3.2 Abstract

Determining the direction of an impinging sound or radio wave is a fundamental capability for technologies such as sonar, radar, and satellite communication. Up to now, sound-direction finding has required either multiple signal frequencies or multiple pressure receivers. Inspired by bat species that add Doppler shifts to their biosonar echoes through fast ear motions, we present a source-direction finding paradigm based on a single frequency and a single pressure receiver. Non-rigid ear motions produce complex Doppler signatures that depend on source direction but are difficult to interpret. To demonstrate that deep learning can solve this problem, we have combined a soft-robotic microphone baffle that mimics a deforming bat ear with a CNN for regression. With this integrated cyberphysical setup, we have been able to achieve a direction-finding accuracy of less than 1 degree based on a single baffle motion. Hence, our results demonstrate that deep learning can make complex nonlinear signal transformations accessible.

3.3 Introduction

Determining the direction of an impinging sound or radio wave is a fundamental capability for a broad range of technical application areas such as sonar [108], radar [109], satellite communications [147], and GPS [148]. Since the propagation direction of a wave is a vector, it is most readily determined based on measurements of vector-valued physical quantities directly linked to it. For acoustic waves, for example, the direction of propagation can be determined from measurements of the particle velocity vector [149, 150]. However, while deriving estimates of the wave propagation direction from a related vector quantity is straightforward, obtaining the respective measurements can be complicated. Hence, a frequently used alternative has been to shift the effort from the basic physical measurement to the estimation stage. For acoustic waves, this is being done by measuring sound pressure, i.e., a simple scalar quantity that can be determined by a conventional microphone. Since estimating a direction vector from a single scalar value is an ill-posed problem, the missing information has to be filled in by using multiple measurements. These additional measurements are typically either acquired along the spatial or the frequency dimension. To obtain more measurements along the spatial dimension, multiple microphones are used to form an array [151]. In human hearing, binaural estimation of the horizontal angle of a sound source follows this approach [152]. Alternatively, a single receiver can be moved in space to collect signals from different positions at different times as is the case in synthetic aperture sonar and radar (SAS, SAR [153, 154]). Along the frequency dimension, multiple measurements can be obtained by analyzing input amplitudes for different frequencies. In human hearing, this is the case for determining the direction of a sound source in elevation [155]. Hence, telling the direction of a sound source from scalar pressure measurements currently requires either multiple receivers or multiple signal frequencies. Both of these approaches have drawbacks. Multiple signal frequencies can only be used if the source produces them. Working

with multiple receivers increases system size and power requirements both at the sensor and the computational stage of the array. Because of these drawbacks, the work presented here has investigated the possibility of a novel paradigm that is based on a single receiver and a single signal frequency.

The single receiver - single frequency paradigm explored here has been inspired by the biosonar sensing system of bats. Bats are small flying mammals that have to be highly parsimonious in terms of the number of emitting and receiving elements as well as computing power. Bat biosonar is limited to one emitter (mouth or nose) and two receivers for ultrasound. Their brain mass is typically less than one gram [156]. To get around these constraints, bat species with sophisticated biosonar systems have evolved interfaces for sound reception, i.e., outer ears (pinnae) that have higher degrees of static as well as dynamic complexity than can be found in engineered sonar systems [1, 69, 157, 158, 159]. Bat pinnae have static complexity in their geometry which includes overall shape as well as local shape features such as grooves and ridges. The pinnae also have dynamic complexity, because they are actuated by an intricate musculature that allows the bats to change the shape of their pinnae during echo reception. Furthermore, these shape changes are associated with surface velocities that are large enough to cause nonlinear effects, i.e., Doppler shifts in the echoes that are transferred from the pinna to the ear canal ([1], Fig. 3.1A).

The hypothesis underlying the current work is that the dynamic, nonlinear complexity results in encoding of additional sensory information, esp. on source direction, that can be used to overcome the limitations of the traditional direction-finding paradigms. There are two challenges to investigating this hypothesis and making use of this additional information: (i) replicating the dynamic geometric complexity and (ii) interpreting the complex nonlinear signals.

Here, a solution to these problems is presented that makes use of a combination of soft

robotics and deep learning. A soft-robotic biomimetic receiver is used to replicate the dynamics of the bat pinna and a deep neural network is used to interpret the signal patterns created. Besides testing the specific hypothesis regarding the existence of a single frequency - single receiver paradigm for finding the direction of a sound source, this work is intended to explore the idea of soft robotics and deep learning to recreate and deal with biological complexity.

3.4 Materials and Methods

3.4.1 Experimental Setup

The geometry of the biomimetic pinna was derived from the pinna shapes of hipposiderid bats and the closely related rhinolophid bats based on micro CT scans of biological specimens [160]. The specimen shapes were simplified by removing geometrical detail below the scale of the employed wavelengths as well as local disruptions of the overall pinna's symmetry. The pinna shape was scaled to a total length of 5.8 cm, i.e., about twice the size in the animals and cast in silicone (Ecoflex, Smooth-On, Inc., Macungie, PA, USA). It was interfaced with a capacitive MEMS microphone (Momimic, Dodotronic, Rome, Italy) to record the received ultrasonic signals via an artificial ear canal (length 9 mm, diameter 4 mm).

The pinna deformations were actuated by a DC servo motor (Maxon RE25 and HEDL encoder combo, Maxon Motors, Switzerland). To couple the pinna and the motor, a cam (length 4.6 cm) was mounted onto the motor shaft and its free end connected to the pinna tip with a string. Rotating the cam about the motor shaft hence resulted in deformation of the pinna by pulling its tip downwards and sideways. The tip achieved maximum speeds of about 3 m/s and maximum displacements of about 4 cm. The pinna model and its deformation

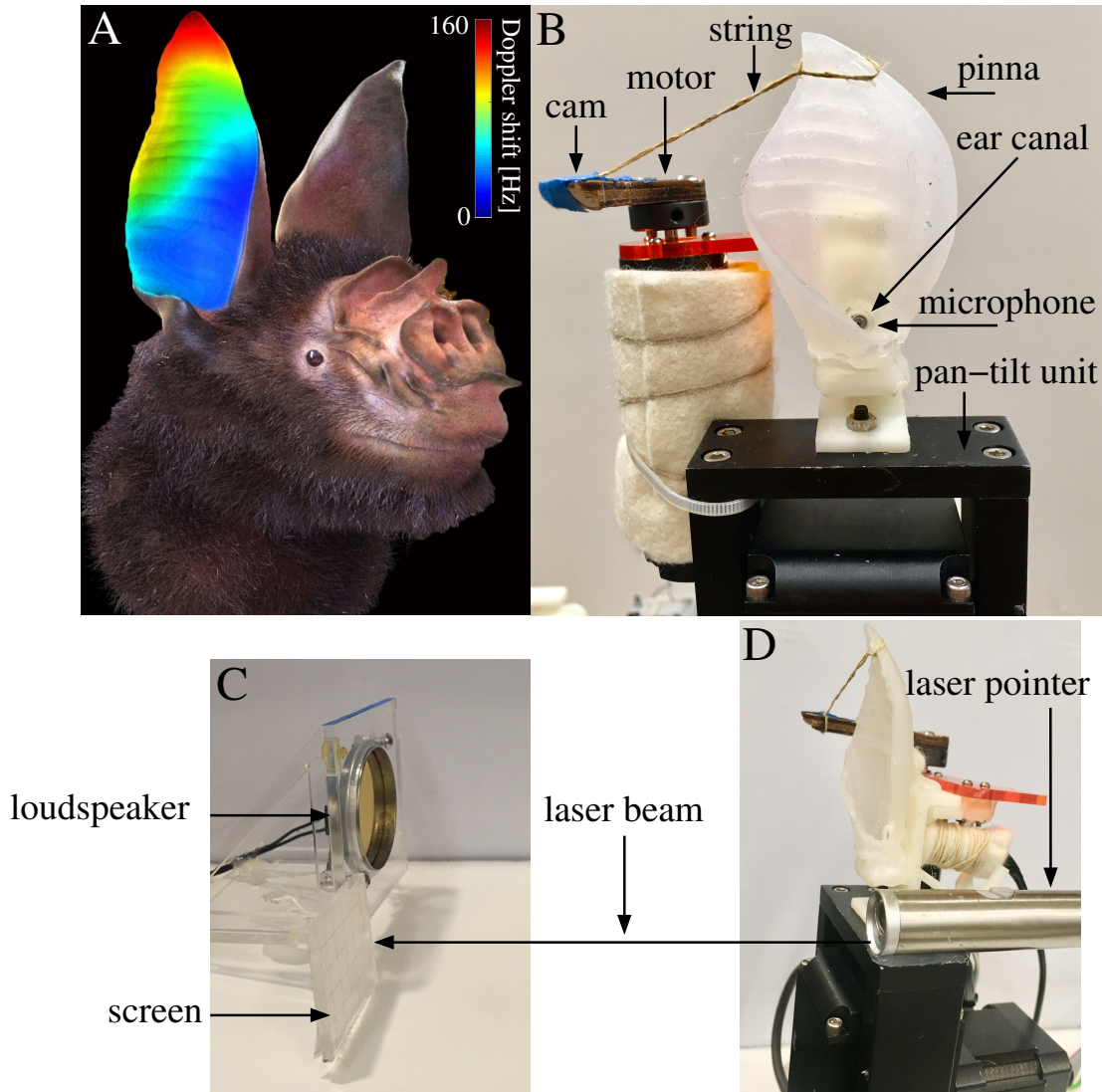


Figure 3.1: **Experimental setup:** A) Biological inspiration from the Doppler shifts produced on the surface of a bat pinna (Pratt's roundleaf bat, *Hipposideros pratti*). Doppler shift amplitudes were derived from the velocities of the pinna surface relative to the propagation direction of the incoming ultrasonic wave are color-coded on the pinna surface [1]. B) Biomimetic silicone pinna mounted on a pan-tilt unit used to orientate the setup for direction sampling and source tracking. The pinna is deformed by a servo motor via a cam and string attached at the pinna tip. C) electrostatic loudspeaker with a screen attached for quantifying the alignment of the pinna with the speaker. D) biomimetic pinna mounted on a pan-tilt-unit with a laser pointer to indicate the orientation of the pinna aperture.

mechanism were mounted on a pan-tilt unit (PTU-46-17.5, FLIR Systems, Inc., Burlington, ON, Canada) that was used to create rotations that covered 180° in azimuth and 60° in elevation. For collection of the training, validation, and testing data, these direction ranges were both sampled in steps of 3° , resulting in 61 different values for azimuth, 21 for elevation, and hence a total of 1,281 unique sampled directions across both dimensions.

An electrostatic loudspeaker (Series 600 open face ultrasonic transducer, SensComp, Livonia, MI, USA) was used to emit ultrasonic pulses that served as input signals from a distance of 50 cm. The pulses had a constant carrier frequency of 90 kHz and a duration of 250 ms. Each pulse was gated by raised-cosine envelope. The pulse signals were converted to analog with a sampling rate of 500 kHz and a resolution of 16 bits (PXIe-6356 data acquisition board, National Instruments, Austin, TX, USA). The pulse emissions and the pinna deformations were synchronized so that two pinna-deformation cycles (period length about 100 ms) were completed during each pulse reception.

3.4.2 Data Preprocessing

The ultrasonic signals received by the capacitive microphone mounted in the ear canal of the biomimetic pinna were digitized with a sampling frequency of 500 kHz and a resolution of 16 bits (PXIe-6356 data acquisition board, National Instruments, Austin, TX, USA). Each recording had a duration of 250 ms and hence contained 125,000 samples. The recorded signals were transformed into spectrogram time-frequency representations using short-time Fourier transforms with a 5500-point Hann window and 0% overlap. The spectrograms were clipped along the frequency axis to the region that contained all expected Doppler shifts (from -1 to 1 kHz). The result was square matrix (22×22) with normalized power-spectral-density values that served as input to the DNN estimator.

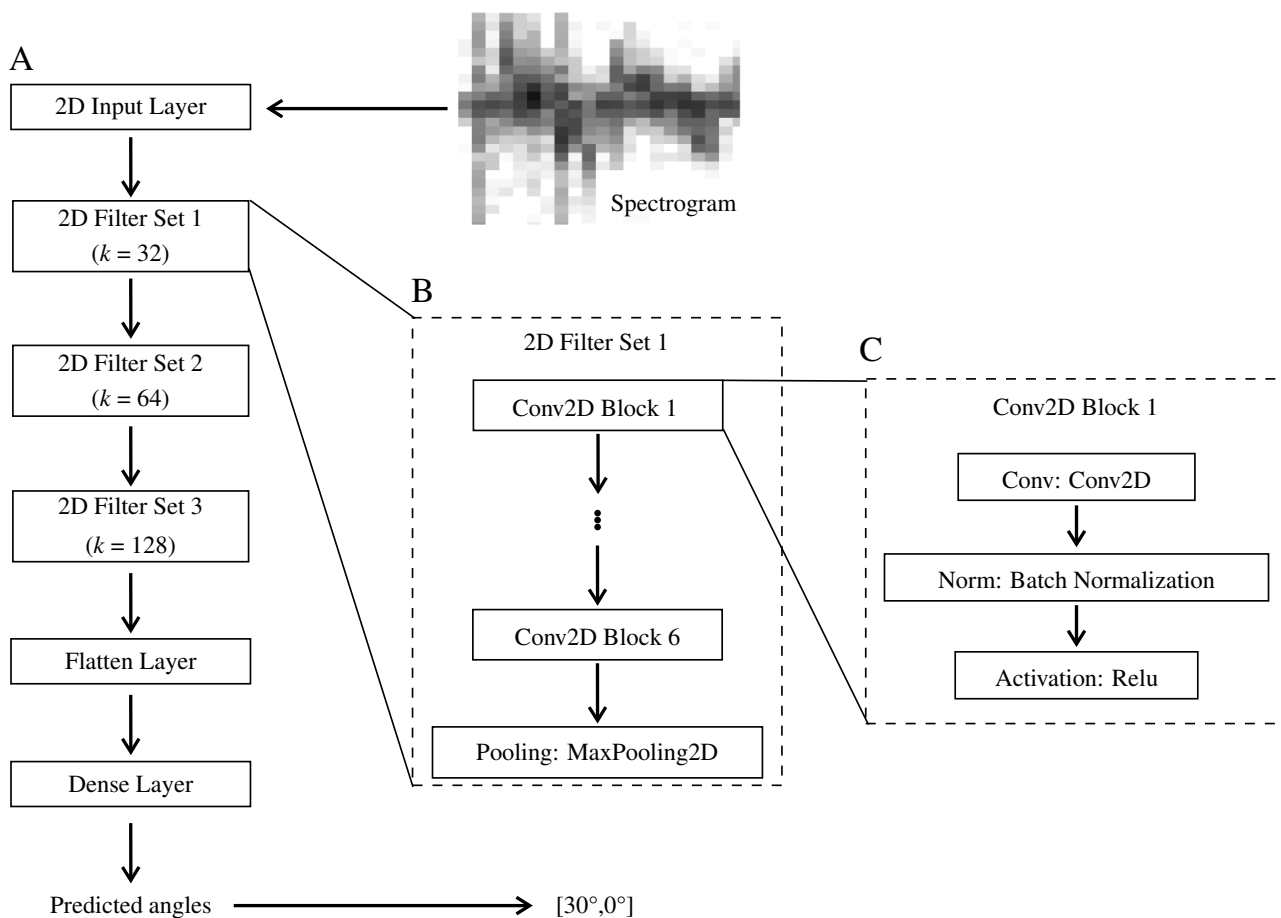


Figure 3.2: **Diagram of the CNN architecture:** A) overall CNN architecture, B) filter set, C) convolution block. The number of different convolution kernels in each filter set is denoted by k .

3.4.3 Convolutional Neural Network Training

A convolutional neural network (CNN) was used for solving the direction-estimation problem. The architecture of the network (Fig. 3.2) was inspired by a DNN for image-based regression, i.e., estimating the value of a continuous variable from images [161] that was in turn based on the VGG CNN architecture that has been designed for image recognition [162]. The network contained a total of 18 convolution layers. In each of these layers, a two-dimensional convolution was followed by batch normalization and a ReLU activation function. The convolution layers were organized into three sets containing six layers each. Each set of

convolution filters had its own number of different filters (32, 64, and 128). The CNN had 1,067,874 parameters in total. Of these parameters, 1,065,186 were trainable (convolution layers 1,061,472, normalization layers 2,688, fully dense layer 1,026) and the remaining 2,688 (mean and variance parameters of the normalization layers) were fixed. A Xavier Glorot uniform initialization was used to assign initial values to the parameters and mean-squared-error served as a loss function. Parameter values were adjusted during training using the Adam algorithm [163] with an initial learning rate of 0.01 and a moderate decay of 0.0001 of the learning rate per epoch number. The batch size was set to 32 throughout. The CNN was implemented using the Keras library running on top of the TensorFlow library. The entire data set of 25,620 recorded Doppler signatures was split into 85% (21,777 signatures) training data, $\sim 13.8\%$ (3,543 signatures) validation data, and $\sim 1.2\%$ (300 points) testing data.

3.4.4 Direction Estimation Testing

To test the direction estimation with hardware in the loop, a laser pointer was attached to the pan-tilt unit and aligned with the normal of the pinna aperture (Fig. 3.1D). To assess how well the output of the CNN was able to align the pinna with the direction of sound source, a screen with a square grid (grid pitch 6.5 mm, size 34 \times 38 mm) was mounted next to the loudspeaker (Fig. 3.1C). The distance between loudspeaker and pinna was kept at 50 cm as was the case for the collection of the training data. At the beginning of each experiment, pinna and loudspeaker were aligned so that the laser beam pointed at the loudspeaker's screen while the pan-tilt unit was oriented to the center of its azimuth range (0°). After this initial alignment, the pan-tilt unit was rotated to one of 61 test positions that were evenly distributed from -90° to 90° in azimuth. For each of the resulting loudspeaker directions, a single ultrasonic input signal was recorded. A simple linear, feed-forward controller was

then used to drive the pan-tilt unit and rotate the pinna in the estimated direction of the sound source. The direction error was then estimated from the position of the laser point on the screen that was attached to the loudspeaker.

3.5 Results

3.5.1 Doppler-shift Signature Associated With Different Directions

The motions of the soft-robotic pinna were found to generate Doppler shifts that were commensurate with the associated velocities, i.e., Doppler shifts up to 800 Hz for speeds up to 3 m/s and 90 kHz carrier frequency. The variability in the velocities across the pinna surface as well as over time resulted in complicated Doppler signatures that were picked up by the microphone in the ear canal of the biomimetic pinna (Fig. 3.3). Qualitative inspection of these signatures gave an impression of distinct patterns associated with different directions and also suggested a certain level of repeatability, i.e., patterns obtained in repeated trials conducted with the same direction of sound incidence tended to resemble each other.

3.5.2 Deep Learning of Direction Finding from Doppler Signatures

The deep regression network was able to learn the direction-finding task based on the Doppler signatures and reached a terminal rms validation error value of around 0.5° within 100 epochs (Fig. 3.4A, validation error 0.67° and training error 0.51° at 100 epochs). The network that achieved the lowest validation error 0.55° at 100 epochs was able to perform on a test data set of 300 signals that had neither been used in training nor in validation with an 0.46° in

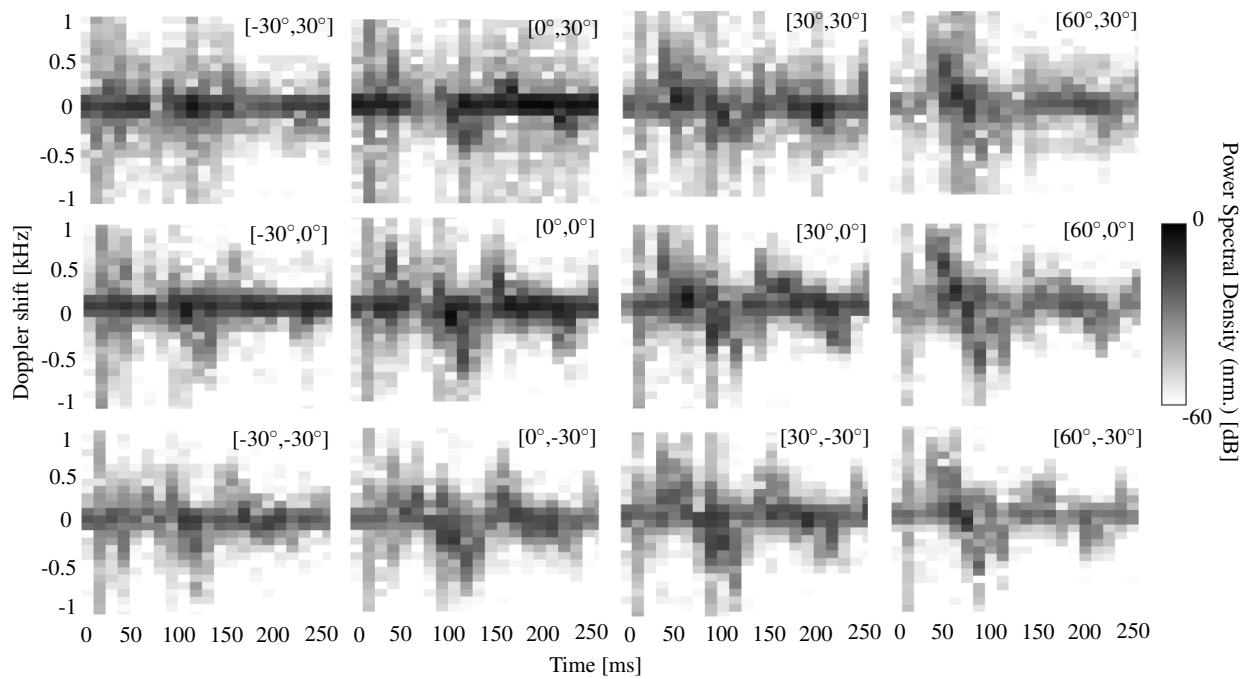


Figure 3.3: **Doppler shift signatures associated with different directions:** Normalized spectrograms of ultrasonic signals received from directions ranging over 90° in azimuth and 60° in elevation. The direction associated with each spectrogram is given as [azimuth, elevation] in the respective panel. The frequency axis of the spectrogram has been centered at the emitted frequency and hence directly gives the value of the Doppler shift.

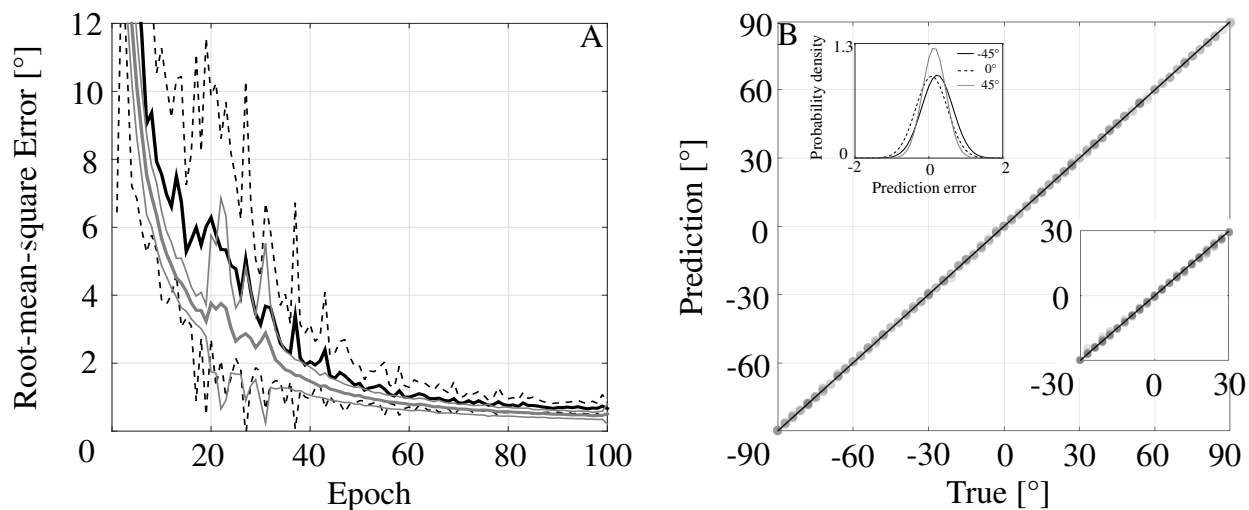


Figure 3.4: **Deep learning of direction finding from Doppler signatures:** A) training and validation loss; B) prediction results. All errors (training, validation, and prediction) were quantified as a root-mean-square error. The averages for training (thick black solid line) and validation losses (thick gray solid line) were based on 20 repetitions of the learning process. The standard deviations in this sample are indicated by thin dashed black lines and thin gray lines respectively. After training, the prediction accuracy of the network was tested with 300 inputs. Prediction results are given for azimuth (main graph) and elevation (lower inset). To further characterize the variability of the estimates as a function of the true direction, fits of Gaussian distributions to the prediction values for three different true azimuth values (-45° , 0° , 45° , $N=21, 23, 23$ respectively pooled from the five nearest directions).

azimuth and 0.56° in elevation (Fig. 3.4B, The az and el errors are significantly different (t -test, $N=300$, $p=3.74E-09$)).

3.5.3 Accuracy of Direction Finding with the Dynamic Soft-robotic Pinna

Testing the DNN direction estimator in an online loop that included the pinna hardware and a pan-tilt unit for source-tracking confirmed the results obtained offline (Fig. 3.5). The rms prediction error for the DNN operating in this experiment was 0.7° (standard deviation

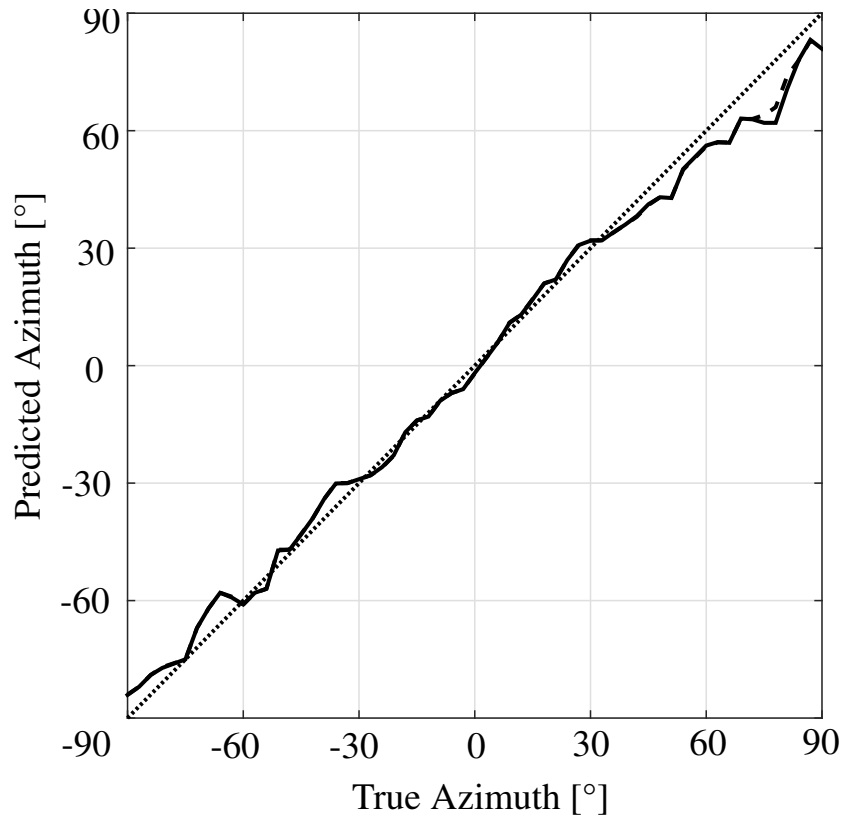


Figure 3.5: **Accuracy of direction finding with a dynamic soft-robotic pinna:** The ability of the soft-robotic pinna mounted on a pan-tilt unit to track a sound source in azimuth was assessed in two different ways: (i) by virtue of the azimuth value that was predicted by the DNN (dashed line) and (ii) by the pointing direction of a laser pointed mounted on the pinna (solid line). Perfect predictions are indicated as a reference (dotted line). The soft-robotic pinna was presented with ultrasound signals from $N=61$ different directions in azimuth.

4.6°). The laser pointer mounted alongside the pinna was able to track the sound source with an rms error of 0.9° (standard deviation 4.9°). The difference between the rms errors for estimation only and laser pointer orientation were not significantly different (t -test, $N=61$, $p=0.86$).

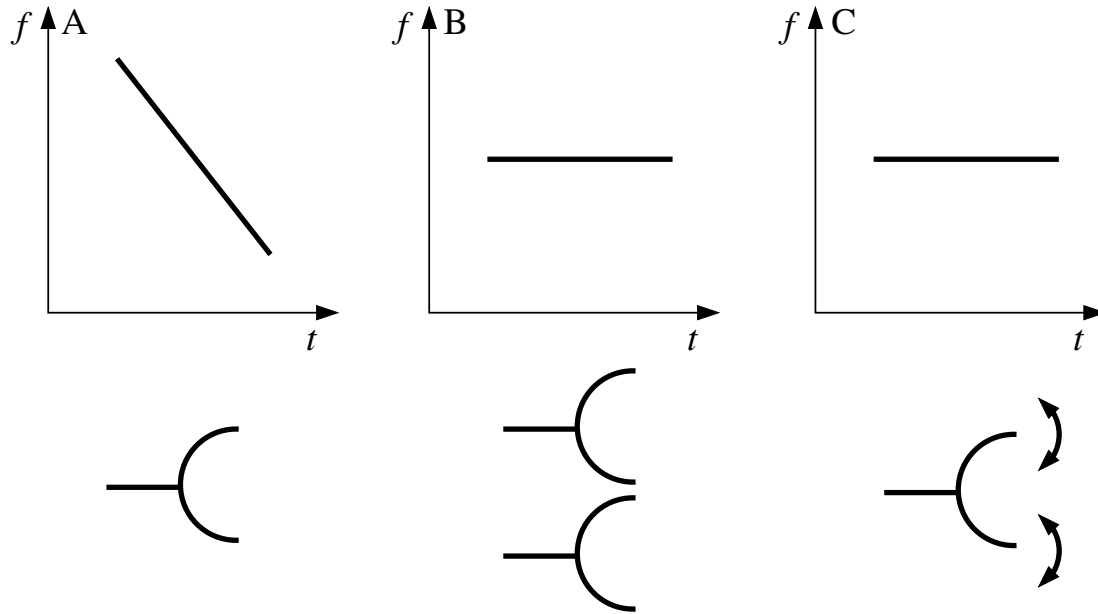


Figure 3.6: **Direction-finding paradigms:** A) single sensor with multiple frequencies, B) single frequency with multiple sensors, C) single frequency with a single dynamic sensor.

3.6 Discussion

The results presented here demonstrate a novel paradigm for finding the direction of a wave source that does away with the need of having either multiple frequencies or multiple receivers (Fig. 3.6). It achieves this by introducing nonlinear complexity into the input signals. In the current incarnation of the paradigm, this has been achieved by virtue of the dynamic geometrical complexity of soft robotics and the resulting signal complexity has been mastered using deep learning.

It remains to be seen how much geometrical and signal complexity is required to reach the current level of direction-finding performance or how much further optimization could be possible. Irrespective of future insights into these questions, the current results demonstrate that deep-learning methods can be a good match for biomimetic complexity as they can turn a complex soft-robotic sensor into a useful direction-finding device without the need to

develop a quantitative understanding of the relationship between the complexities of sensor behavior and the encoded information.

The direction-finding performance achieved here ($\sim 0.5^\circ$) compares very favorably with what has been reported for bats and humans so far: The acuity of human observers for localizing sound in the vertical has been estimated as 12° (monaurally) and 9° (binaurally) [164]. For a bat species not known for fast pinna motions or exploiting Doppler shifts (big brown bat, *Eptesicus fuscus*), the acuity for separating pairs of horizontal rods in the vertical plane was found to be 3° [40]. Another study of the same bat species has reported a tracking accuracy of 1.6° in the horizontal plane [46]. Replicating direction finding in big brown bats based on compressed external ear transfer functions with a fully-connected, three-layer backpropagation network has achieved accuracies of 7.5° in azimuth and 8.9° in elevation [165].

The higher accuracy achieved here could be explained by two non-mutually exclusive hypotheses: First, the human and bat experiments could have contained additional sources of variability that degraded their results. Second, bat species with fast ear motions could have access to better sensory information than humans and big brown bats. The second hypothesis could be tested by performing direction-finding experiments with rhinolophid or hipposiderid bats. If such experiments were successful, the results presented here could make a contributions to a better understanding of the diversity in bat biosonar function beyond the introduction of a general sensing paradigm.

Chapter 4

Summary and Conclusions

4.1 Major Findings

I have developed a soft robotic to investigate the functionality of the fast ear motion of some bat species. In the first part, I have completed the animal experiments to prove that the Doppler shift generated by the fast ear motion will enter into the ear canal, hence to constitute a nonlinear mechanism for the active encoding of sensory information. In the second part, I have developed a soft robotic to mimicked the fast ear motion to able to achieve the sound source direction finding based on the Doppler shift signatures. I have then developed a novel biomimetic nonlinear sensing paradigm by integrating deep learning and soft robotics. The detailed findings are:

- The fastest pinna tip motion speed recorded in the lab environment is $\sim 2.2 \text{ m/s}$ that gives a Doppler shift of 383 Hz which is more than seven times the Doppler shift compensation threshold (50 Hz).
- The highest speeds occurred in a region along the outer pinna rim that was a good match for where the orientations of the velocity vectors at maximum speed were close to parallel to the direction of sound radiation.
- All echoes in echolocation sequences accompanied by pinna motions contain Doppler-shift signatures that should be perceivable by the bats.

- The time-frequency Doppler signatures were direction-dependent and could hence be used to obtain information on the direction of a biosonar target.
- Fast pinna motions constitute a previously unknown second source of self-generated Doppler shifts which could constitute a nonlinear mechanism for the active encoding of sensory information.
- A deep regression network was able to learn the direction-finding task based on the Doppler signatures and reached a terminal rms validation error value of around 0.5° within 100 epochs.
- Tested the DNN direction estimator in an online loop that included the pinna hardware and a pan-tilt unit for source-tracking confirmed the results obtained offline
- Established a novel paradigm for finding the direction of a wave source that needs a single frequency with a single dynamic sensor
- Demonstrated a good example of the integration of deep learning and soft robotics for a biomimetic nonlinear sensing paradigm.

4.2 Discussion

Two types of pinna motions have been found for Horseshoe bats and Old World leaf-nosed bats: rigid and non-rigid [69]. The non-rigid motion causes substantial changes in the ear structure to compare to the rigid one [69]. Pinna motions in the horseshoe and hipposiderid bats could serve the animals' sensing in different ways: (i) a rigid component that reorients the beampattern [70], (ii) a non-rigid, linear component that changes the pinna's beampattern by the pinna geometry. The rigid component can be easily understood as a scanning

operation where the most sensitive coverage of the beampattern is re-pointed in different directions. The non-rigid, linear motion components have been demonstrated to enhance the encoding of sensory information related to direction-finding [71]. Changing the pinna geometry to produce a different beampattern shape can be seen as an alternative to change the frequency for a fixed pinna geometry [146]. The non-linear transformations due to the pinna-generated Doppler shifts described here add an additional feature to the pinna motions in bats. It remains to be determined if the Doppler-transformations of the echoes serve a functional purpose in those animals. If they are an integral part of the peripheral dynamics of the bats' biosonar system, as the evidence presented here suggests, this would mean that the bats can harness nonlinear effects that could lead to new functional principles for enhance sensing of natural environments and enable engineered sensory systems with the same capabilities.

The results obtained from the soft robotics demonstrate a novel paradigm for finding the direction of a wave source that does away with the need of having either multiple frequencies [155] or multiple receivers [151]. This abolishes previous limitations on what was technologically feasible, which was achieved by introducing nonlinear complexity into the input signals. This achievement implies that bioinspired robotics is a generic approach that not only brings new insight into the engineering area but also provides a novel way to help understand and explain the biological world. For example, the spring-loaded inverted pendulum (SLIP) model was used to study walking dynamics and gait transitions between walking and running [166] and a mobile robot employing insect strategies for navigation [167].

The accomplishments achieved in this research were only possible because the dynamic geometrical complexity of soft robotics and the resulting signal complexity has been comprehended using deep learning techniques. And similar success has been found at analyzing complex single-molecule emission patterns [168] and analyzing fringe patterns [169] with deep

learning. Without deep learning, it would have been extremely hard to decipher the complex Doppler signatures generated by the irregular, non-stationary geometry of the biomimetic pinna. Hence, the results presented in this dissertation served as a great example of how biomimetic soft-robotics and deep learning can be integrated. Our study demonstrates that deep learning can make complex nonlinear signal transformations accessible. Related success include a vision-based robotic grasping system using deep learning for 3D object recognition and pose estimation [170] and a deep learning algorithm for visual-based robot navigation [171]

The direction-finding performance achieved here ($\sim 0.5^\circ$) compares very favorably with what has been reported for bats and humans so far [40, 46, 164, 165]. One of the hypotheses is that bat species with fast ear motions could have access to better sensory information than humans and big brown bats. This hypothesis could be tested by performing direction-finding experiments with rhinolophid or hipposiderid bats. If such experiments were successful, the results presented here could make a contribution to a better understanding of the diversity in bat biosonar function beyond the introduction of a general sensing paradigm.

4.3 Suggestions for Future Work

- It remains to be seen how much geometrical and signal complexity is required to reach the current level of direction-finding performance or how much further optimization could be possible.
- The hypothesis that bat species with fast ear motions could have access to better sensory information than humans and big brown bats could be tested by performing direction-finding experiments with rhinolophid or hipposiderid bats.

Bibliography

- [1] X. Yin and R. Müller. Fast-moving bat ears create informative doppler shifts. *Proc. Natl. Acad. Sci. U.S.A.*, 116(25):12270–12274, 2019.
- [2] D. R. Griffin. Listening in the dark: the acoustic orientation of bats and men. 1958.
- [3] C. F. Moss and H. U. Schnitzler. Behavioral studies of auditory information processing. In *Hearing by Bats*, pages 87–145. Springer, 1995.
- [4] D. Wirth and D. Reeder. *Mammal Species of the World: A Taxonomic and Geographic Reference*, volume 1. Baltimore, MD, 2005.
- [5] J. Fjeldså and N. Krabbe. Birds of the high andes: a manual to the birds of the temperate zone of the andes and patagonia. *South America*, 1990.
- [6] M. Johnson, P. T. Madsen, W. M. Zimmer, N. Aguilar de Soto, and P. L. Tyack. Beaked whales echolocate on prey. *Proc. Royal Soc. B.*, 271(suppl_6):S383–S386, 2004.
- [7] A. Kaveh and N. Farhoudi. A new optimization method: Dolphin echolocation. *Adv. Eng. Softw.*, 59:53–70, 2013.
- [8] N. B. Simmons, K. L. Seymour, J. Habersetzer, and G. F. Gunnell. Primitive early eocene bat from wyoming and the evolution of flight and echolocation. *Nature*, 451(7180):818–821, 2008.
- [9] S. Sterbing-D’Angelo, M. Chadha, C. Chiu, B. Falk, W. Xian, J. Barcelo, all J. M. Zook, and C. F. Moss. Bat wing sensors support flight control. *Proc. Natl. Acad. Sci. U.S.A.*, 108(27):11291–11296, 2011.

- [10] S. Greif and B. M. Siemers. Innate recognition of water bodies in echolocating bats. *Nat. Commun.*, 1(1):1–6, 2010.
- [11] Alex Salinas. Night flying missions vs. mexican free-tailed bats - twenty million tiny bats living 11 miles from randolph pose a giant risk to base aircraft, 2013.
- [12] R. Müller. Dynamics of biosonar systems in horseshoe bats. *Eur. Phys. J. - Spec. Top.*, 224(17-18):3393–3406, 2015.
- [13] Ilana E. Strauss. 7 surprising facts about bats, 2016.
- [14] C. Chiu, W. Xian, and C. F. Moss. Flying in silence: echolocating bats cease vocalizing to avoid sonar jamming. *Proc. Natl. Acad. Sci. U.S.A.*, 105(35):13116–13121, 2008.
- [15] A. J. Corcoran and W. E. Conner. Bats jamming bats: food competition through sonar interference. *Science*, 346(6210):745–747, 2014.
- [16] N. Orange and N. Abaid. A transfer entropy analysis of leader-follower interactions in flying bats. *Eur. Phys. J. Spec. Top.*, 224(17):3279–3293, 2015.
- [17] Y. Lin, N. Abaid, and R. Müller. Bats adjust their pulse emission rates with swarm size in the field. *J. Acoust. Soc. Am.*, 140(6):4318–4325, 2016.
- [18] J. Fullard and J. Dawson. The echolocation calls of the spotted bat *euderma maculatum* are relatively inaudible to moths. *J. Exp. Biol.*, 200(1):129–137, 1997.
- [19] M.B. Fenton, P.A. Faure, and J.M. Ratcliffe. Evolution of high duty cycle echolocation in bats. *J. Exp. Biol.*, 215(17):2935–2944, 2012.
- [20] M. B. Fenton, C. V. Portfors, I. L. Rautenbach, and J. M. Waterman. Compromises: sound frequencies used in echolocation by aerial-feeding bats. *Can. J. Zool.*, 76(6):1174–1182, 1998.

- [21] S. Rosen and P. Howell. *Signals and Systems for Speech and Hearing*, volume 29. Brill, 2011.
- [22] A. Surlykke and E. K. Kalko. Echolocating bats cry out loud to detect their prey. *PLoS one*, 3(4):e2036, 2008.
- [23] G. Koay, H. E. Heffner, and R. S. Heffner. Audiogram of the big brown bat (*Eptesicus fuscus*). *Hearing research*, 105(1):202–210, 1997.
- [24] N. P. Van Nguyen, L. Tang, F. Hasan, N. D. Minh, and S. Mukhopadhyay. Nature-inspired sensor system for vital signs detection. *Sens. Actuator A Phys.*, 281:76–83, 2018.
- [25] G. Jones and M. W. Holderied. Bat echolocation calls: adaptation and convergent evolution. *Proc. Royal Soc. B.*, 274(1612):905–912, 2007.
- [26] N.B. Simmons. *Mammal Species of the World: A Taxonomic and Geographic Reference*, volume 1, chapter Order Chiroptera, pages 312–529. Johns Hopkins University Press, 3rd edition, 2005.
- [27] H. U. Schnitzler, C. F. Moss, and A. Denzinger. From spatial orientation to food acquisition in echolocating bats. *Trends in Ecology & Evolution*, 18(8):386–394, 2003.
- [28] G. von der Emde and H. U. Schnitzler. Classification of insects by echolocating greater horseshoe bats. *J. Comp. Physiol.*, 167(3):423–430, 1990.
- [29] B. Tian and H. U. Schnitzler. Echolocation signals of the greater horseshoe bat (*Rhinolophus ferrumequinum*) in transfer flight and during landing. *J. Acoust. Soc. Am.*, 101(4):2347–2364, 1997.
- [30] T. Kingston and S. J. Rossiter. Harmonic-hopping in wallacea’s bats. *Nature*, 429(6992):654–657, 2004.

- [31] E. K. Kalko and H. U. Schnitzler. Plasticity in echolocation signals of european pipistrelle bats in search flight: implications for habitat use and prey detection. *Behav. Ecol. Sociobiol.*, 33(6):415–428, 1993.
- [32] A. Salles, C. A. Diebold, and C. F. Moss. Echolocating bats accumulate information from acoustic snapshots to predict auditory object motion. *Proc. Natl. Acad. Sci. U.S.A.*, 2020.
- [33] C. F. Moss, C. Chiu, and A. Surlykke. Adaptive vocal behavior drives perception by echolocation in bats. *Curr. Opin. Neurobiol.*, 21(4):645–652, 2011.
- [34] A. Surlykke and C. F. Moss. Echolocation behavior of big brown bats, *ptesicus fuscus*, in the field and the laboratory. *J. Acoust. Soc. Am.*, 108(5):2419–2429, 2000.
- [35] K. Ghose and C. F. Moss. Steering by hearing: a bat’s acoustic gaze is linked to its flight motor output by a delayed, adaptive linear law. *J. Neurosci.*, 26(6):1704–1710, 2006.
- [36] K. Ghose and C. F. Moss. The sonar beam pattern of a flying bat as it tracks tethered insects. *J. Acoust. Soc. Am.*, 114(2):1120–1131, 2003.
- [37] F. A. Webster and O. G. Brazier. Experimental studies on target detection, evaluation, and interception by echolocating bats. Technical report, SENSORY SYSTEMS LAB TUCSON ARIZ, 1965.
- [38] W. M. Masters, A. J. Moffat, and J. A. Simmons. Sonar tracking of horizontally moving targets by the big brown bat *ptesicus fuscus*. *Science*, 228(4705):1331–1333, 1985.
- [39] L. Harten, A. Katz, A. Goldshtein, M. Handel, and Y. Yovel. The ontogeny of a mammalian cognitive map in the real world. *Science*, 369(6500):194–197, 2020.

- [40] B. D. Lawrence and J. A. Simmons. Echolocation in bats: The external ear and perception of the vertical positions of targets. *Science*, 218(4571):481–483, 1982.
- [41] J.A. Simmons, S. A. Kick, B. D. Lawrence, C. Hale, C. Bard, and B. Escudie. Acuity of horizontal angle discrimination by the echolocating bat, *Eptesicus fuscus*. *J. Comp. Physiol.*, 153(3):321–330, 1983.
- [42] G. D. Pollak. Time is traded for intensity in the bat’s auditory system. *Hearing research*, 36(2-3):107–124, 1988.
- [43] D. E. Valentine and C. F. Moss. Spatially selective auditory responses in the superior colliculus of the echolocating bat. *J. Neurosci.*, 17(5):1720–1733, 1997.
- [44] H. Hartridge. Acoustic control in the flight of bats. *Nature*, 156(3965):490–494, 1945.
- [45] J. A. Simmons. The resolution of target range by echolocating bats. *J. Acoust. Soc. Am.*, 54(1):157–173, 1973.
- [46] W. M. Masters, A. J. Moffat, and J. A. Simmons. Sonar tracking of horizontally moving targets by the big brown bat *Eptesicus fuscus*. *Science*, 228(4705):1331–1333, 1985.
- [47] T. C. Williams, L. C. Ireland, and J. M. Williams. High altitude flights of the free-tailed bat, *tadarida brasiliensis*, observed with radar. *Journal of Mammalogy*, 54(4):807–821, 1973.
- [48] X.Tian, J. Iriarte-Diaz, K. Middleton, R. Galvao, E. Israeli, A. Roemer, A. Sullivan, A. Song, S. Swartz, and K. Breuer. Direct measurements of the kinematics and dynamics of bat flight. *Bioinspir. Biomim.*, 1(4):S10, 2006.
- [49] J. Murray. *Bats*. Big Buddy Books, 2019.

- [50] S. M. Swartz, M. S. Groves, H. D. Kim, and W. R. Walsh. Mechanical properties of bat wing membrane skin. *J. Zool.*, 239(2):357–378, 1996.
- [51] K. L. Marshall, M. Chadha, L. A. deSouza, S. J. Sterbing-D’Angelo, C. F. Moss, and E. A. Lumpkin. Somatosensory substrates of flight control in bats. *Cell Rep.*, 11(6):851–858, 2015.
- [52] H. R. Erwin, W. W. Wilson, and C. F. Moss. A computational sensorimotor model of bat echolocation. *J. Acoust. Soc. Am.*, 110(2):1176–1187, 2001.
- [53] NB N. B. Simmons. Mammal species of the world: A taxonomic and geographic reference, edited by de wilson & dm reeder, 2005.
- [54] P. Kounitsky, J. Rydell, E. Amichai, A. Boonman, O. Eitan, A. J. Weiss, and Y. Yovel. Bats adjust their mouth gape to zoom their biosonar field of view. *Proc. Natl. Acad. Sci. U.S.A.*, 112(21):6724–6729, 2015.
- [55] R. Kuc. Bat noseleaf model: echolocation function, design considerations, and experimental verification. *J. Acoust. Soc. Am.*, 129(5):3361–3366, 2011.
- [56] L. Feng, L. Gao, H. Lu, and R. Müller. Noseleaf dynamics during pulse emission in horseshoe bats. *PloS one*, 7(5):e34685, 2012.
- [57] W. He, S. C. Pedersen, A. K. Gupta, J. A. Simmons, and R. Müller. Lancet dynamics in greater horseshoe bats, *Rhinolophus ferrumequinum*. *PLoS One*, 10(4):e0121700, 2015.
- [58] N. Matsuta, S. Hiryu, E. Fujioka, Y. Yamada, H. Riquimaroux, and Y. Watanabe. Adaptive beam-width control of echolocation sounds by cf–fm bats, *Rhinolophus ferrumequinum nippon*, during prey-capture flight. *Journal of Experimental Biology*, 216(7):1210–1218, 2013.

- [59] N. H. Fletcher. *Acoustic Systems in Biology*. Oxford University Press, 1992.
- [60] D. J. Hartley and R. A. Suthers. The sound emission pattern and the acoustical role of the noseleaf in the echolocating bat, *Carollia perspicillata*. *J. Acoust. Soc. Am.*, 82(6):1892–1900, 1987.
- [61] Q. Zhuang and R. Müller. Numerical study of the effect of the noseleaf on biosonar beamforming in a horseshoe bat. *Phys. Rev. E*, 76(5):051902, 2007.
- [62] W. He, S. Pedersen, A.K. Gupta, J.A. Simmons, and R. Müller. Lancet dynamics in greater horseshoe bats, *Rhinolophus ferrumequinum*. *PLOS ONE*, 10(4):e0121700, April 2015.
- [63] A. K. Gupta, D. Webster, and R. Müller. Interplay of lancet furrows and shape change in the horseshoe bat noseleaf. *J. Acoust. Soc. Am.*, 138(5):3188–3194, 2015.
- [64] C. Csorba, P. Ujhelyi, and N. Thomas. *Horseshoe Bats of the World*. Alana Books, Bishop’s Castle, Shropshire, UK, 2003.
- [65] H. Schneider and F. P. Möhres. Die ohrbewegungen der hufeisenfledermäuse (*Chiroptera, Rhinolophidae*) und der mechanismus des bildhörens. *Z. Vgl. Physiol.*, 44(1):1–40, 1960.
- [66] D.R. Griffin, D.C. Dunning, D.A. Cahlander, and F.A. Webster. Correlated orientation sounds and ear movements of horseshoe bats. *Nature*, 4860(1185-1188), December 1962.
- [67] J.D. Pye, M. Flinn, and A. Pye. Correlated orientation sounds and ear movements of horseshoe bats. *Nature*, 196:1186–1188, 1962.
- [68] J.D. Pye and L.H. Roberts. Ear movements in a hipposiderid bat. *Nature*, 225:285–286, January 1970.

- [69] X. Yin, P. Qiu, L. Yang, and R. Müller. Horseshoe bats and old world leaf-nosed bats have two discrete types of pinna motions. *J. Acoust. Soc. Am.*, 141(5):3011–3017, 2017.
- [70] V. A. Walker, H. Peremans, and J. C. T. Hallam. One tone, two ears, three dimensions: A robotic investigation of pinnae movements used by rhinolophid and hipposiderid bats. *J. Acoust. Soc. Am.*, 104(1):569–79, July 1998.
- [71] R. Müller, A.K. Gupta, H. Zhu, M. Pannala, U.S. Gillani, Y. Fu, P. Caspers, and J.R. Buck. Dynamic substrate for the encoding sensory information in bat biosonar. *Phys. Rev. Lett.*, 118(15):158102, April 2017.
- [72] H. Schneider and F. P. Möhres. Die Ohrbewegungen der Hufeisennasenfledermäuse (Chiroptera, Rhinolophidae) und der Mechanismus des Bildhörens. *Z. Vergl. Physiol.*, 44(1):1–40, January 1960.
- [73] L. Gao, S. Balakrishnan, W. He, Z. Yan, and R. Müller. Ear deformations give bats a physical mechanism for fast adaptation of ultrasonic beampatterns. *Phys. Rev. Lett.*, 107(21):214301, November 2011.
- [74] X. Yin, P. Qiu, L. Yang, and R. Müller. Horseshoe bats and old world leaf-nosed bats have two discrete types of pinna motions. *J. Acoust. Soc. Am.*, 141(5):3011–3017, May 2017.
- [75] F.P. Möhres. Über die Ultraschallorientierung der Hufeisennasen (Chiroptera-Rhinolophinae). *J. Comp. Physiol. A*, 34(6):547–588, 1953.
- [76] J. Mogdans, J. Ostwald, and H.-U. Schnitzler. The role of pinna movement for the localization of vertical and horizontal wire obstacles in the greater horseshoe bat, *Rhinolopus ferrumequinum*. *J. Acoust. Soc. Am.*, 84(5):1676–9, November 1988.

- [77] R. Müller. Quantitative approaches to sensory information encoding by bat noseleaves and pinnae. *Can. J. Zool.*, 96:79–86, January 2018.
- [78] H.-U. Schnitzler. Control of Doppler shift compensation in the greater horseshoe bat, *Rhinolophus ferrumequinum*. *J. Comp. Physiol. A*, 82(1):79–92, 1973.
- [79] A.J. Corcoran and C.F. Moss. Sensing in a noisy world: lessons from auditory specialists, echolocating bats. *J. Exp. Biol.*, 220(24):4554–4566, 2017.
- [80] J.D. Pye. A theory of echolocation by bats. *J. Laryngol. Otol.*, 74(10):718–729, 1960.
- [81] S. Zhang, L. Zhang, R. Zhang, and R. Müller. The relationship between pinna and noseleaf motions in hipposiderid bats. *J. Acoust. Soc. Am.*, 141(5):3485–3485, 2017.
- [82] L. Zhang, R. Zhang, S. Zhang, L. Yang, and R. Müller. Noseleaf motions impart dynamic signatures on bat biosonar pulses. *J. Acoust. Soc. Am.*, 142(4):2664–2664, 2017.
- [83] L. Yang, A. Yu, and R. Müller. Design of a dynamic sonar emitter inspired by hipposiderid bats. *Bioinspir. Biomim.*, 13(5):056003, 2018.
- [84] L. Yang and R. Müller. Differential entropy analysis of the acoustic characteristics of a biomimetic dynamic sonar emitter. *Symmetry*, 12(3):391, 2020.
- [85] L. Zhang, L. Yang, R. Zhang, and R. Müller. An experimental link between fast noseleaf deformations and biosonar pulse dynamics in hipposiderid bats. *J. Acoust. Soc. Am.*, 148(2):954–961, 2020.
- [86] X. Yin, P. Qiu, and R. Müller. Quantification of fast pinna motions in rhinolophid and hipposiderid bats. *J. Acoust. Soc. Am.*, 142(4):2664–2664, 2017.

- [87] P. Qiu and R. Müller. Variability in the rigid pinna motions of hipposiderid bats and their impact on sensory information encoding. *J. Acoust. Soc. Am.*, 147(1):469–479, 2020.
- [88] M. J. Bender, M. McClelland, G. Bledt, A. Kurdila, T. Furukawa, and R. Mueller. Trajectory estimation of bat flight using a multi-view camera system. In *AIAA Modeling and Simulation Technologies Conference*, page 1806, 2015.
- [89] M. J. Bender, H. M. McClelland, A. Kurdila, and R. Mueller. Recursive bayesian estimation of bat flapping flight using kinematic trees. In *AIAA Modeling and Simulation Technologies Conference*, page 0945, 2016.
- [90] M. Bender, J. Guo, N. Powell, A. Kurdila, and R. Müller. Learning bioinspired joint geometry from motion capture data of bat flight. *Bioinspir. Biomim.*, 14(3):036013, 2019.
- [91] T. Y. Hubel, D. K. Riskin, S. M. Swartz, and K.S. Breuer. Wake structure and wing kinematics: the flight of the lesser dog-faced fruit bat, *cynopterus brachyotis*. *J. Exp. Biol.*, 213(20):3427–3440, 2010.
- [92] A. Hedenström and L. C. Johansson. Bat flight: aerodynamics, kinematics and flight morphology. *J. Exp. Biol.*, 218(5):653–663, 2015.
- [93] T. L. Hedrick. Software techniques for two-and three-dimensional kinematic measurements of biological and biomimetic systems. *Bioinspir. Biomim.*, 3(3):034001, 2008.
- [94] A. Mathis, P. Mamidanna, K. M. Cury, T. Abe, V. N. Murthy, M. W. Mathis, and M. Bethge. Deeplabcut: markerless pose estimation of user-defined body parts with deep learning. *Nat. Neurosci.*, 21(9):1281–1289, 2018.

- [95] W. Zhang and M. M. Yartsev. Correlated neural activity across the brains of socially interacting bats. *Cell*, 178(2):413–428, 2019.
- [96] A. J. Bergou, S. Swartz, K. Breuer, and G. Taubin. 3d reconstruction of bat flight kinematics from sparse multiple views. In *2011 IEEE International Conference on Computer Vision Workshops (ICCV Workshops)*, pages 1618–1625. IEEE, 2011.
- [97] A. J. Bergou, S. M. Swartz, H. Vejdani, D. K. Riskin, L. Reimnitz, G. Taubin, and K. S. Breuer. Falling with style: bats perform complex aerial rotations by adjusting wing inertia. *PLoS Biol.*, 13(11):e1002297, 2015.
- [98] J. A. Cheney, D. Ton, N. Konow, D. K. Riskin, K. S. Breuer, and S. M. Swartz. Hindlimb motion during steady flight of the lesser dog-faced fruit bat, *cynopterus brachyotis*. *Plos one*, 9(5):e98093, 2014.
- [99] J. Iriarte-Díaz and S. M. Swartz. Kinematics of slow turn maneuvering in the fruit bat *cynopterus brachyotis*. *J. Exp. Biol.*, 211(21):3478–3489, 2008.
- [100] J. Iriarte-Díaz, D. K. Riskin, D. J. Willis, K. S. Breuer, and S. M. Swartz. Whole-body kinematics of a fruit bat reveal the influence of wing inertia on body accelerations. *J. Exp. Biol.*, 214(9):1546–1553, 2011.
- [101] D. K. Riskin, D. J. Willis, J. Iriarte-Díaz, T. L. Hedrick, M. Kostandov, J. Chen, D. H. Laidlaw, K. S. Breuer, and S. M. Swartz. Quantifying the complexity of bat wing kinematics. *J. Theor. Biol.*, 254(3):604–615, 2008.
- [102] M. A. Hopkins, D. W. Hong, and A. Leonessa. Compliant locomotion using whole-body control and divergent component of motion tracking. In *2015 IEEE International Conference on Robotics and Automation (ICRA)*, pages 5726–5733. IEEE, 2015.

- [103] M. Sun. Insect flight dynamics: stability and control. *Rev. Mod. Phys.*, 86(2):615, 2014.
- [104] J. J. Socha. Gliding flight in the paradise tree snake. *Nature*, 418(6898):603–604, 2002.
- [105] S. M. Swartz and N. Konow. Advances in the study of bat flight: the wing and the wind. *Can. J. Zool.*, 93(12):977–990, 2015.
- [106] G. V. Lauder. Fish locomotion: recent advances and new directions. *Ann. Rev. Mar. Sci.*, 7:521–545, 2015.
- [107] J. Sutlive, A. Singh, S. Zhang, and R. Mueller. A biomimetic soft robotic pinna for emulating dynamic reception behavior of horseshoe bats. *Bioinspir. Biomim.*, 2020.
- [108] R.E. Hansen and N.Z. Kolev. *Sonar Systems*, chapter Introduction to synthetic aperture sonar, pages 1–28. INTECH Open Access, London, UK, 2011.
- [109] F. Athley, C. Engdahl, and P. Sunnergren. On radar detection and direction finding using sparse arrays. *IEEE Trans. Aerosp. Electron. Syst.*, 43(4):1319–1333, 2007.
- [110] D. P. Skinner, R. A. Altes, and J. D. Jones. Broadband target classification using a bionic sonar. *J. Acoust. Soc. Am.*, 62(5):1239–1246, 1977.
- [111] M. I. Skolnik. Introduction to radar systems, 3rdmcgraw-hill. *New York*, 2002.
- [112] N. Riopelle, P. Caspers, and D. Sofge. Terrain classification for autonomous vehicles using bat-inspired echolocation. In *2018 International Joint Conference on Neural Networks*, pages 1–6. IEEE, 2018.
- [113] W. Gao and M. Hinders. Mobile robot sonar backscatter algorithm for automatically distinguishing walls, fences, and hedges. *Int. J. Robot.*, 25(2):135–145, 2006.

- [114] J. S. Pan, T. K. Dao, and T. T. Nguyen. A compact bat algorithm for unequal clustering in wireless sensor networks. *Applied Sciences*, 9(10):1973, 2019.
- [115] S. Goyal and M. S. Patterh. Modified bat algorithm for localization of wireless sensor network. *Wirel. Pers. Commun.*, 86(2):657–670, 2016.
- [116] E. Tuba, M. Tuba, and D. Simian. Range based wireless sensor node localization using bat algorithm. In *Proceedings of the 13th ACM Symposium on Performance Evaluation of Wireless Ad Hoc, Sensor, & Ubiquitous Networks*, pages 41–44, 2016.
- [117] S. Goyal and M. S. Patterh. Performance of bat algorithm on localization of wireless sensor network. *Int. J. Comput. Appl.*, 6(3):351–358, 2013.
- [118] M. R. Sathya and M. M. T. Ansari. Load frequency control using bat inspired algorithm based dual mode gain scheduling of pi controllers for interconnected power system. *Int. J. Electr. Power Energy Syst.*, 64:365–374, 2015.
- [119] M. Sharawi, E. Emary, I. A. Saroit, and H. El-Mahdy. Bat swarm algorithm for wireless sensor networks lifetime optimization. *Int. J.*, 3(5):654–664, 2014.
- [120] R. J. Wood. The first takeoff of a biologically inspired at-scale robotic insect. *IEEE Trans. Robot.*, 24(2):341–347, 2008.
- [121] W. Shyy, H. Aono, S. K. Chimakurthi, P. Trizila, C. K. Kang, C. E. Cesnik, and H. Liu. Recent progress in flapping wing aerodynamics and aeroelasticity. *Prog. Aerosp. Sci.*, 46(7):284–327, 2010.
- [122] A. Ramezani, X. Shi, S. J. Chung, and S. Hutchinson. Bat bot (b2), a biologically inspired flying machine. *2016 IEEE ICRA*, pages 3219–3226, 2016.

- [123] S. J. Furst, G. Bunget, and S. Seelecke. Design and fabrication of a bat-inspired flapping-flight platform using shape memory alloy muscles and joints. *Smart Mater. Struct.*, 22(1):014011, 2012.
- [124] J. W. Bahlman, S. M. Swartz, and K. S. Breuer. Design and characterization of a multi-articulated robotic bat wing. *Bioinspir. Biomim.*, 8(1):016009, 2013.
- [125] M. A. Woodward and M. Sitti. Multimo-bat: A biologically inspired integrated jumping–gliding robot. *Int. J. Robot.*, 33(12):1511–1529, 2014.
- [126] S. J. Chung and M. Dorothy. Neurobiologically inspired control of engineered flapping flight. *J. Guid. Control Dyn.*, 33(2):440–453, 2010.
- [127] G. Schuller, K. Beuter, and H.-U. Schnitzler. Response to frequency shifted artificial echoes in the bat *Rhinolophus ferrumequinum*. *J. Comp. Physiol.*, 89:275–286, 1974.
- [128] J.A. Simmons. Response of the Doppler echolocation system in the bat, *Rhinolophus ferrumequinum*. *J. Acoust. Soc. Am.*, 56(2):672–682, 1974.
- [129] U. Heilmann. *Das Frequenzunterscheidungsvermögen bei der großen Hufeisennase, Rhinolophus ferrumequinum*. PhD thesis, Tübingen University, 1984.
- [130] H.-U. Schnitzler. *Localization and Orientation in Biology and Engineering*, chapter The Performance of Bat Sonar Systems, pages 211–224. Springer Verlag, Berlin, Heidelberg, New York, Tokyo, 1984.
- [131] J.Y. Bouguet and P. Perona. Camera calibration from points and lines in dual-space geometry. In *5th European Conference on Computer Vision, Freiburg, Germany*, 1998.
- [132] J.F. Hughes. *Computer Graphics: Principles and Practice*. Addison-Wesley, Upper Saddle River, New Jersey, 3rd edition, 2014.

- [133] K.-G. Heller and O.v. Helversen. Resource partitioning of sonar frequency bands in rhinolophoid bats. *Oecologia*, 80(2):178–186, 1989.
- [134] G. Schuller. Echo delay and overlap with emitted orientation sounds and doppler-shift compensation in the bat, *Rhinolophus ferrumequinum*. *J. Comp. Physiol. A*, 114(1):103–114, 1977.
- [135] U. v. Luxburg. A tutorial on spectral clustering. *Statistics and Computing*, 17(4):395–416, 2007.
- [136] J. Shi and J. Malik. Normalized cuts and image segmentation. *IEEE Trans. Pattern Anal. Mach. Intell.*, 22(8):888–905, 2000.
- [137] I. Bürk. Spectral clustering. Bachelor thesis, University of Stuttgart, 2012.
- [138] G. Jones and E. C. Teeling. The evolution of echolocation in bats. *Trends Ecol. Evol.*, 21(3):149–56, March 2006.
- [139] G. Jones and J.M.V. Rayner. Foraging behavior and echolocation of wild horseshoe bats *rhinolophus ferrumequinum* and *r. hipposideros* (chiroptera, rhinolophidae). *Behav. Ecol. Sociobiol.*, 25(3):183–191, 1989.
- [140] S. Hiryu, K. Katsura, L.K. Lin, H. Riquimaroux, and Y. Watanabe. Doppler-shift compensation in the taiwanese leaf-nosed bat (*hipposideros terasensis*) recorded with a telemetry microphone system during flight. *J. Acoust. Soc. Am.*, 118(6):3927–3933, 2005.
- [141] J.R. Buck. Information theoretic bounds on source localization performance. *Proc. IEEE SAM Workshop*, pages 184–188, 2002.
- [142] V. Bruns and E. Schmieszek. Cochlear innervation in the greater horseshoe bat: Demonstration of an acoustic fovea. *Hear. Res.*, 3:27–43, 1980.

- [143] H.-U. Schnitzler and J. Ostwald. Adaptations for the detection of fluttering insects by echolocation in horseshoe bats. In J.P. Ewert, R.R. Capranica, and D.I. Ingle, editors, *Advances in Vertebrate Neuroethology*, pages 801–827. Plenum Press, New York, NY, 1983.
- [144] H.-U. Schnitzler and A. Denzinger. Auditory fovea and Doppler shift compensation: adaptations for flutter detection in echolocating bats using cf-fm signals. *J. Comp. Physiol. A*, 197(5):541–559, 2011.
- [145] R. Müller and H.-U. Schnitzler. Acoustic flow perception in cf-bats: properties of the available cues. *J. Acoust. Soc. Am.*, 105(5):2958–2966, May 1999.
- [146] A.K. Gupta, D. Webster, and R. Müller. Entropy analysis of frequency and shape change in horseshoe bat biosonar. *Phys. Rev. E*, 97:062402, June 2018.
- [147] T. E. Tuncer and B. Friedlander. *Classical and Modern Direction-of-Arrival Estimation*. Academic Press, Cambridge, MA, 2009.
- [148] H. M. Peng, E. R. Chang, and L. S. Wang. Rotation method for direction finding via gps carrier phases. *IEEE Trans. Aerosp. Electron. Syst.*, 36(1):72–84, 2000.
- [149] A. Nehorai and E. Paldi. Acoustic vector-sensor array processing. *IEEE Trans. Signal Process.*, 42(9):2481–2491, 1994.
- [150] H. E. De Bree. The microflown: An acoustic particle velocity sensor. *Acoust. Aust.*, 31(3):91–94, 2003.
- [151] J. Benesty, J. Chen, and Y. Huang. *Microphone Array Signal Processing*, volume 1. Springer Science & Business Media, Berlin, Germany, 2008.
- [152] J. C. Middlebrooks and D. M. Green. Sound localization by human listeners. *Annu. Rev. Psychol.*, 42(1):135–159, 1991.

- [153] M. P. Hayes and P. T. Gough. Synthetic aperture sonar: A review of current status. *IEEE J. Ocean. Eng.*, 34(3):207–224, 2009.
- [154] A. Moreira, P. Prats-Iraola, M. Younis, G. Krieger, I. Hajnsek, and K. P. Papathanassiou. A tutorial on synthetic aperture radar. *IEEE Geosci. Remote Sens. Mag.*, 1(1):6–43, 2013.
- [155] B. Zonooz, E. Arani, K. P. Kording, P. R. Aalbers, T. Celikel, and A. J. Van Opstal. Spectral weighting underlies perceived sound elevation. *Sci. Rep.*, 9(1):1–12, 2019.
- [156] B. K. McNab and M. Köhler. The difficulty with correlations: energy expenditure and brain mass in bats. *Comp. Biochem. Physiol. Part A Mol. Integr. Physiol.*, 212:9–14, 2017.
- [157] L. Gao, S. Balakrishnan, W. He, Z. Yan, and R. Müller. Ear deformations give bats a physical mechanism for fast adaptation of ultrasonic beam patterns. *Phys. Rev. Lett.*, 107(21):214301, 2011.
- [158] R. Müller, H. Lu, and J. R. Buck. Sound-diffracting flap in the ear of a bat generates spatial information. *Phys. Rev. Lett.*, 100(10):108701, 2008.
- [159] R. Müller. A numerical study of the role of the tragus in the big brown bat. *J. Acoust. Soc. Am.*, 116(6):3701–3712, 2004.
- [160] J. Sutlive and R. Müller. Dynamic echo signatures created by a biomimetic sonar head. *Bioinspir. Biomim.*, 14(6):066014, 2019.
- [161] S. Lathuilière, P. Mesejo, X. Alameda-Pineda, and R. Horaud. A comprehensive analysis of deep regression. *IEEE Trans. Pattern Anal. Mach. Intell.*, 42(9):2065–2081, 2020.

- [162] K. Simonyan and A. Zisserman. Very deep convolutional networks for large-scale image recognition. In *Proc. 3th Int. Conf. Learning Representations*. ICLR, 2015.
- [163] D. P. Kingma and J. Ba. Adam: A method for stochastic optimization. In *Proc. 3th Int. Conf. Learning Representations*. ICLR, 2015.
- [164] S. R. Oldfield and S. P. Parker. Acuity of sound localisation: a topography of auditory space. iii. monaural hearing conditions. *Perception*, 15(1):67–81, 1986.
- [165] J. M. Wotton and R. L. Jenison. A backpropagation network model of the monaural localization information available in the bat echolocation system. *J. Acoust. Soc. Am.*, 101(5):2964–2972, 1997.
- [166] R. Blickhan, A. Seyfarth, H. Geyer, S. Grimmer, H. Wagner, and M. Günther. Intelligence by mechanics. *Philos. Trans. R. Soc. A.*, 365(1850):199–220, 2007.
- [167] D. Lambrinos, R. Möller, T. Labhart, R. Pfeifer, and R. Wehner. A mobile robot employing insect strategies for navigation. *Rob. Auton. Syst.*, 30(1-2):39–64, 2000.
- [168] P. Zhang, S. Liu, A. Chaurasia, D. Ma, M. J. Mlodzianoski, E. Culurciello, and F. Huang. Analyzing complex single-molecule emission patterns with deep learning. *Nat. Methods*, 15(11):913–916, 2018.
- [169] S. Feng, Q. Chen, G. Gu, T. Tao, L. Zhang, Y. Hu, W. Yin, and C. Zuo. Fringe pattern analysis using deep learning. *Advanced Photonics*, 1(2):025001, 2019.
- [170] J. Yu, K. Weng, G. Liang, and G. Xie. A vision-based robotic grasping system using deep learning for 3d object recognition and pose estimation. In *2013 IEEE International Conference on Robotics and Biomimetics (ROBIO)*, pages 1175–1180. IEEE, 2013.

- [171] W. Chen, T. Qu, Y. Zhou, K. Weng, G. Wang, and G. Fu. Door recognition and deep learning algorithm for visual based robot navigation. In *2014 IEEE International Conference on Robotics and Biomimetics (ROBIO 2014)*, pages 1793–1798. IEEE, 2014.

Appendices

Appendix A

Matlab Code for Spectrogram

Extraction

```
1 %% This Matlab script is used to compute the spectrogram of a waveform ...
   recording.
2 %% The epectrograms are cropped to the expected range of the Doppler
3 %% shifts (emitted frequency +/- 1 kHz).
4 %% The cropped spectrograms serve as input to the CNN estimator.
5
6 % Author: Xiaoyan Yin
7 % Mechanical Engineering, Virginia Tech
8 % email: xiaoyan6@vt.edu
9 % Feb 2019; Last revision: 23-Nov-202
10
11 % Each recording (acqdata) contains 125,000 samples (recording
12 % duration: 250 ms, sampling rate: 500 kHz)
13 % The output (DopplerShift) is a 22-by-22 matrix representing the
14 % cropped spectrogram.
15
16 %----- BEGIN CODE -----
17
18 %% Load data from file
```

```

19 acqdata = load(' ../data/Recording.mat ', 'acqdata1 ')
20 acqdata = struct2cell(acqdata);
21 acqdata = cell2mat(acqdata);
22
23 %% High-pass filter (removes low-frequency noise)
24 fc = 10000; % Cut-off frequency
25 fs = 500000; % Sampling rate
26 [b,a] = butter(6,fc/(fs/2), 'high'); % Butterworth filter of order 6
27 acqdata = filtfilt(b,a,acqdata); % Apply the filter
28
29 %% Compute the spectrogram with a 5,500-point Hann window and 0% overlap
30 [S,F,T,P]=spectrogram(acqdata, hanning(5500), 0, 5500, 500000, 'yaxis');
31
32 % Normalize the power - spectral - density values by the maximum taken over
33 % the entire spectrogram
34 NorPSD = P./max(P(:));
35
36 % Convert to logarithmic power spectral density [dB scale]
37 LogNorPSD=10*log10(NorPSD);
38
39 % Crop to the frequency region of possible Doppler shifts (from -1 kHz to ...
    1kHz around emitted frequency)
40 DopplerShift = [];
41 for i = 1001 : -1 : 980,
42     DopplerShift = [DopplerShift; LogNorPSD(i,:)];
43 end
44
45 % Plot the Doppler shift spectrogram
46 figure(1)
47 sf = surf(T*1000,F(980:1001,1)-90000,DopplerShift)
48 colorbar

```

```
49 colormap(jet);
50 sf.EdgeColor = 'none';
51 view(0,90)
52 caxis ([-60,-0]);
53 xlim([5.5,236.5])
54 ylim([-1000,900])
55 grid on
56 xlabel('Time (ms)')
57 ylabel('Doppler shift (Hz)')
58 title('Spectrogram')
59
60 % save the resulting plot to a PNG file
61 saveas(figure(1),'../results/Spectrogram.png')
62
63 %----- END OF CODE -----
```

Appendix B

Python Code for CNN Training

```
1 # -*- coding: utf-8 -*-
2 """
3 Created on Sun Aug  2 15:37:56 2020
4
5 @author: Xiaoyan Yin
6 """
7 # Import the necessary packages
8 from tensorflow import keras
9 from keras.optimizers import Adam
10 from sklearn.model_selection import train_test_split
11 import pandas as pd
12 import numpy as np
13 import math
14 import matplotlib.pyplot as plt
15 import scipy.io as spio
16 from keras.callbacks import Callback
17 from keras.layers.normalization import BatchNormalization
18 from keras.layers.convolutional import Conv2D
19 from keras.layers.convolutional import MaxPooling2D
20 from keras.layers.core import Activation
21 from keras.layers.core import Dense
22 from keras.layers import Flatten
```

```
23 from keras.layers import Input
24 from keras.models import Model
25
26 # Prepare the input data and labels (supervised learning)
27 #input_data = "../data/sample-data.txt"
28 mat = spio.loadmat(r'../data/DATA.mat') #load mat file
29 PosData = mat['DATA'] #position data
30 # Normalize the input dataset
31 MinValue = PosData.min()
32 NorPosData = [x - MinValue for x in PosData]
33 NorPosData = np.array(NorPosData)
34 MaxValue = NorPosData.max()
35 NorPosData = NorPosData/MaxValue
36 # Rearrange the dataset structure
37 DATA = np.zeros((25620,22,22), dtype="float")
38 for i in range(0, 25619 + 1):
39     T = NorPosData[:, :, i]
40     DATA[i, :, :] = T
41 DATA = np.reshape(DATA,(25620,22,22,1))
42 # Load label dataset
43 label = pd.read_csv('../data/Label.csv')
44 label = np.array(label)
45 # Normalize the label data
46 label = label/180
47
48 # Split the data into 3 parts: training, validation and testing
49 split = train_test_split(label, DATA, test_size=0.15, random_state=42)
50 (trainAttrX, otherAttrX, trainImagesX, otherImagesX) = split
51
52 split = train_test_split(otherAttrX, otherImagesX, test_size=0.9219, ...
    random_state=42)
```

```

53 (testAttrX, valAttrX, testImagesX, valImagesX) = split
54
55 # Build the training model
56 def create_cnn(width, height, depth, filters=(32, 64, 128), regress=False):
57     # initialize the input shape and channel dimension, assuming
58     # TensorFlow/channels-last ordering
59     inputShape = (height, width, depth)
60     chanDim = -1
61     # define the model input
62     inputs = Input(shape=inputShape)
63     # loop over the number of filters
64     for (i, f) in enumerate(filters):
65         # if this is the first CONV layer then set the input
66         # appropriately
67         if i == 0:
68             x = inputs
69         # CONV => BN => RELU=> POOL
70         x = Conv2D(f, (3, 3), padding="same")(x);
71         x = BatchNormalization(axis=chanDim)(x)
72         x = Activation("relu")(x)
73         x = Conv2D(f, (3, 3), padding="same")(x)
74         x = BatchNormalization(axis=chanDim)(x)
75         x = Activation("relu")(x)
76         x = Conv2D(f, (3, 3), padding="same")(x)
77         x = BatchNormalization(axis=chanDim)(x)
78         x = Activation("relu")(x)
79         x = Conv2D(f, (3, 3), padding="same")(x)
80         x = BatchNormalization(axis=chanDim)(x)
81         x = Activation("relu")(x)
82         x = Conv2D(f, (3, 3), padding="same")(x)
83         x = BatchNormalization(axis=chanDim)(x)

```

```
84     x = Activation("relu")(x)
85     x = Conv2D(f, (3, 3), padding="same")(x)
86     x = BatchNormalization(axis=chanDim)(x)
87     x = Activation("relu")(x)
88     x = MaxPooling2D(pool_size=(2, 2))(x)
89     x = Flatten()(x)
90     # check to see if the regression node should be added
91     if regress:
92         x = Dense(2, activation="linear")(x)
93     # construct the CNN
94     model = Model(inputs, x)
95     # return the CNN
96     model.summary()
97     return model
98
99 # Hyperparameter configuration
100 model = create_cnn(22, 22, 1, regress=True) #input size is 22x22
101 opt = Adam(lr=1e-2, decay=1e-2 / 100) #set learning rate and ...
102     decay parameters
103
104 model.compile(loss="mean_squared_error", optimizer=opt) #set loss function
105
106 # Callback for loss logging per epoch
107 class LossHistory(Callback):
108     def on_train_begin(self, logs={}):
109         self.losses = []
110         self.val_losses = []
111         self.train_losses = []
112
113     def on_epoch_end(self, batch, logs={}):
114         self.losses.append(logs.get('loss'))
115         self.val_losses.append(logs.get('val_loss'))
```

```

114         self.train_losses.append(logs.get('train_loss'))
115
116 # Define the training parameters
117 def run_myCNN():
118     history = LossHistory()
119     print("running model...")
120     model.fit(trainImagesX, trainAttrX, validation_data=(valImagesX, ...
121               valAttrX),
122             epochs=100, batch_size=32, callbacks=[history])
123     return history
124
125 # Training
126 history = run_myCNN()
127 # The loss values (mean_squared_error)
128 loss = history.losses
129 val_loss = history.val_losses
130 train_loss = history.losses
131
132 # Predictions (azimuth, elevation) of testing dataset
133 prediction = model.predict(testImagesX)
134
135 # Convert the loss values to RMSE (root-mean squared error) in degree
136 val_loss = np.sqrt(val_loss)*180
137 train_loss = np.sqrt(train_loss)*180
138
139 #convert the prediction values to degree
140 prediction = prediction*180
141
142 # Get RMSE values of the predictions for both azimuth and elevation
143 Truth = testAttrX*180 #True values in degree
144 Diff = Truth - prediction #Difference between truth and prediciton
145 RMSEA = math.sqrt(sum(Diff[0:299,0]*Diff[0:299,0])/300) #RMSE of azimuth

```

```
144 RMSEE = math.sqrt(sum(Diff[0:299,1]*Diff[0:299,1])/300) #RMSE of elevation
145
146 # plot the prediction of the testing dataset
147 #azimuth
148 fig = plt.figure()
149 ax = fig.add_subplot(111)
150 x1,y1 = [0,180],[0,180]
151 plt.plot(x1,y1)
152 plt.plot(Truth[:,0],prediction[:,0], 'r*')
153 plt.xlabel('True (degree)')
154 plt.ylabel('Prediction (degree)')
155 plt.title('Prediction of azimuth')
156 plt.xlim(0,180)
157 plt.ylim(0,180)
158 plt.grid(True)
159 ax.set_aspect('equal',adjustable='box')
160 # save the resulting plot to a PNG file
161 plt.savefig("../results/prediction_azimuth.png")
162 plt.show()
163 plt.close()
164
165 #elevation
166 fig = plt.figure()
167 ax = fig.add_subplot(111)
168 x2,y2 = [0,60],[0,60]
169 plt.plot(x2,y2)
170 plt.plot(Truth[:,1],prediction[:,1], 'r*')
171 plt.xlabel('True (degree)')
172 plt.ylabel('Prediction (degree)')
173 plt.title('Prediction of elevation')
174 plt.xlim(0,60)
```

```
175 plt.ylim(0,60)
176 plt.grid(True)
177 ax.set_aspect('equal',adjustable='box')
178 # save the resulting plot to a PNG file
179 plt.savefig("../results/prediction_elevation.png")
180 plt.show()
181 plt.close()
182
183 #plot the training and validation loss
184 fig = plt.figure()
185 ax =fig.add_subplot(111)
186 x3 = range(1,101)
187 plt.plot(x3,train_loss ,linestyle='solid',color='r')
188 plt.plot(x3,val_loss ,linestyle='solid',color='b')
189 plt.xlabel('Epoch')
190 plt.ylabel('Root-mean-square Error (degree)')
191 plt.title('Training (red) and validation (blue) losses during learning')
192 plt.xlim(0,100)
193 plt.ylim(0,12)
194 plt.grid(True)
195 # save the resulting plot to a PNG file
196 plt.savefig("../results/TrainingAndValidationLoss.png")
197 plt.show()
198 plt.close()
```